

RAM

● ROBOTICS
AND
MECHATRONICS

CONCEPT DESIGN OF A NOVEL FERROFLUID
BASED FEEDBACK SYSTEM FOR PRIMARY
SYSTEM OF A VERSATILE ENDOVASCULAR
ASSISTING ROBOT
S.S. (Saket) Pradhan

MSC ASSIGNMENT

Committee:

dr. ir. M. Abayazid
dr. G. Dagnino
Dr.-Ing. D. Kundrat
dr. ir. B.J.F. van Beijnum

August, 2022

005RaM2022
Robotics and Mechatronics
EEMCS
University of Twente
P.O. Box 217
7500 AE Enschede
The Netherlands

UNIVERSITY
OF TWENTE.

TECHMED
CENTRE

UNIVERSITY
OF TWENTE.

DIGITAL SOCIETY
INSTITUTE

Concept design of a novel Ferrofluid based feedback system
for a primary system of a versatile endovascular assisting
robot

Saket Pradhan

August 24, 2022

Summary

Cardiovascular diseases (CVDs) are the most common cause of death. Endovascular procedures offer a solution to treating many CVDs. Robot-assisted minimally invasive endovascular surgeries are showing improved accuracy with short patient recovery times and are also being developed such that the surgeons' exposure to ionising radiation during the procedure is eliminated. Developing such teleoperated robots has limitations especially since natural haptic feedback to the surgeon is lost and hence haptic feedback is crucial especially when it comes to endovascular procedures to reduce intra-operative injury.

This thesis introduces a novel concept design for a ferrofluid-based feedback system for a robot-assisted endovascular system. The idea is to provide 3-D tactile feedback for a surgeon such that it enables the surgeon to manipulate a catheter intuitively. The proposed concept is a system which employs ferrofluid, which is a smart fluid, along with powerful electromagnets. It is envisioned to provide direction-based tactile feedback to the surgeon. A few design assumptions were considered to conceptualise the system and to validate these design assumptions a set of experiments were performed. The optimum placement of electromagnets for the system was also determined through two experiments. A user study with 10 volunteers was conducted to provide a proof of concept for the feasibility of the concept design of this system. The test showed a 68% compliance to sensing feedback. Direction-based feedback was accurately reported 44% of the time. The challenges incurred during the user study were listed out and further improvements to the initial design were proposed for a functional prototype. Future scope of the system can be extended to various domains such as the gaming industry where full-body suits filled with ferrofluid can be developed with an array of electromagnets to provide full-body feedback to the user. The concept used here can also be extended to other systems that require 3-D perception of forces.

Contents

1	Introduction	1
1.1	Context	1
1.2	Problem statement	2
1.3	Outline	3
2	Background	4
2.1	Telerobotics	4
2.2	CathBot	4
2.3	Feedback	5
2.4	Smart fluids	5
3	Design	8
3.1	Concept envisioned for ferrofluid based feedback system	8
3.2	Design of Validation experiments	8
3.3	Model design	11
3.4	Plunger	11
4	Experimental Setup	13
4.1	Validation and evaluation Experiments	13
4.2	Model testing	16
4.3	Image Processing	20
4.4	User Study	21
5	Results	26
5.1	Flap elevation test	26
5.2	Evaluation of force exerted by ferrofluid	29
5.3	Model Testing	32
5.4	User Study	34
6	Discussion	39
7	Conclusion	42
7.1	Future works	42
A	Appendix	44
A.1	Volume of ferrofluid and required elevation	46
	Bibliography	59

1 Introduction

1.1 Context

Diseases are defined as a definite pathological process that has a characteristic set of signs and symptoms that affects the part or a whole body without a physical injury (1). If left untreated some diseases also could cause fatality. The most common cause of death is attributed to Cardiovascular diseases (CVD) globally each year (2). CVD is a general term for various conditions affecting the heart or blood vessels. A few predominant CVDs are Ischemic Heart Disease (IHD) and Congestive Heart Failure (CHF). Ischemic Heart Diseases are the problems caused in the heart due to the narrowing of blood vessels and Congestive Heart Failure is a progressive heart illness that affects the hearts ability to pump blood (3). The usual course of treatment for these diseases is prescribing orally ingested medicines or endovascular procedures such as angioplasty.

Endovascular surgeries are *Minimally Invasive Surgeries* (MIS) which are less painful, have



Figure 1.1: The da vinci robotics surgical system used for MIS (4)

smaller incisions and cause less scarring which is preferred by patients. Surgeons also prefer MIS due to lower recovery time and reduced risk of complications (5). While MIS is an attractive option, it limits the field view of the surgeon (6), especially in the case of cardiovascular surgeries as fluroscopy is employed to navigate a catheter. This process exposes the surgeons to higher levels of ionizing radiation

Since the growth of medical robotics in mid-1980s (7) there has been a growing interest in robotic surgeries or robot assisted surgeries. These surgeries typically are achieved by a trained clinician/surgeon who uses a robot to complete the procedure with a higher accuracy than the conventional surgical procedure would achieve. Surgeries performed in this method are termed as minimally invasive robotic surgeries or MIRS. While MIRS is attractive for the shortened patient recovery and hospitalisation times due to less interventional trauma (8), it also intervenes a surgeons direct hand-eye coordination and the surgeon in many cases lacks natural tactile feedback (9).

The recent development depicted in the works of Kundrat *et al* (8) and Abdelaziz *et al* (10) is a novel MR safe endovascular robotic platform that introduces a CathBot as seen in figure 1.2, which is a telerobot consisting of master and slave system. The slave system part of CathBot is in the interventional room with the patient while the master system along with the valve con-

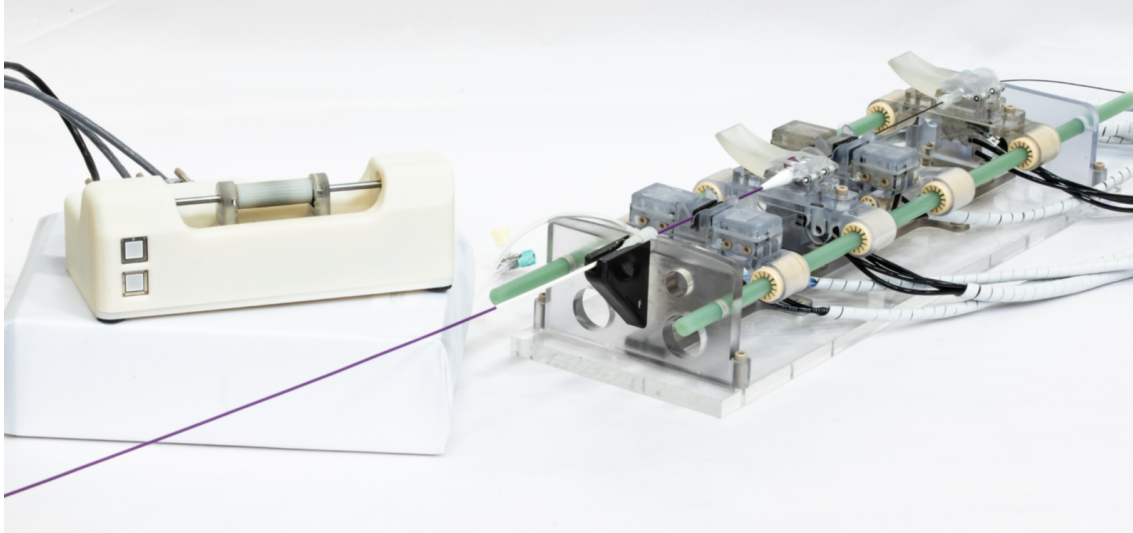


Figure 1.2: CathBot: Master (left) and Slave (right) systems (10)

troller are outside the operating room. The system is designed such that a surgeon is able to control the slave system movements by actuating the master system to perform an endovascular procedure. Section 2.2 provides more information about this system. This system also ensures that the surgeons exposure to radiation is reduced. The telerobot designed in (8) highlights its master design objectives as an *intuitive* and remote manipulation of the master system such that the kinematics mimic conventional manual instrument manipulation which is familiar to clinicians. The feedback system in the master system is reliant on a linear and a rotary motors which provide resistive forces against the intended motion as force feedback to the surgeon. While there exists a force feedback, this feedback is provided only in two *Degrees of Freedom (DoF)*. The position of the catheter within the vasculature is however not received by the surgeon intuitively through this feedback system.

In this thesis **a concept design of a novel ferrofluid based feedback system for a robot assisted endovascular system** is proposed which can be integrated with the master system framework described in (8) and (10) . This section explains the limitations of MIRS, the importance of tactile feedback for a surgeon, goals of the thesis and the outline of the report.

1.2 Problem statement

Haptic feedback is reported as a major limitation by robot-assisted surgeons when it comes to Minimally Invasive Robotic Surgeries (MIRS) (11) since the natural feedback is eliminated. Tactile feedback is required by medical professionals when probing a needle into the tissue to control the pressure applied on the needle. This skill is acquired after training and practical experience. The same feedback must also be replicated when a surgeon/clinician is using a robot to accurately perform the given endovascular procedure. The tactile feedback a surgeon receives from a catheter/guidewire while performing an endovascular surgery enables the surgeon to guide the catheter/guidewire inside the vasculature. In case of the CathBot, motors that provide force feedback can only tell the user that a contact has been made, more information is needed as to which part of the catheter has made contact for quicker position correction and minimizing potential damage during the endovascular process.

To further this goal of providing an intuitive manipulation experience of the master system in this robotic platform I would like to test the use of an alternative haptic feedback mechanism which utilises ferrofluid. Ferrofluid is a smart fluid that changes (generally increases) its viscosity when exposed to a magnetic field. In this assignment, the hypothesis is that the ferrofluid based feedback system would provide a more intuitive knowledge about the position

of the catheter within the vasculature to the user (in this case a surgeon). This ensures that the user(surgeon) receives the feedback in a tactile fashion as well as visual feedback to guide the catheter intuitively. The user(surgeon) would "feel" the catheter as the user(surgeon) is guiding the catheter/guidewire in the vasculature. This kind of feedback is important for the surgeon to accurately anticipate the position of the catheter wire and provide an adequate actuation (either translation or rotational feed) in the required direction based on the "feel", which is provided as feedback by the ferrofluid based feedback system.

1.3 Outline

In the following sections a list of background knowledge required to understand the terminologies and definitions is provided in chapter 2. The envisioned concept design of the ferrofluid based feedback system is discussed in chapter 3. Chapter 4 discusses the various experiments performed. Chapter 5 discusses the results of the experiments. Chapter 6 discusses key observations made throughout the course of various experiments. Chapter 7 concludes the thesis and discusses future works for this system.

2 Background

This section is to familiarize the reader with certain terms used throughout the document. The concept of telerobotics, importance and types of feedback system and a brief introduction to smart fluids such as ferrofluids are discussed in this section. The discussions are merely brief description of the concepts.

2.1 Telerobotics

As described in the works of Sheridan *et al* (12) telerobotics is a form of teleoperation where information such as goals and constraints are communicated as input by a human to a computer and accomplishments, concerns and sensory data are received by the human as output and feedback, while the task is executed by a master-slave robot system. Teleoperation essentially is the extension of an individual's senses and manipulation capabilities to a remote location. A typical teleoperation system consists of three subsystems, namely: The human operator, master-slave manipulator, remote task. as can be seen from the figure 2.1.

The human operator with force feedback and visual cues manipulates the master system by

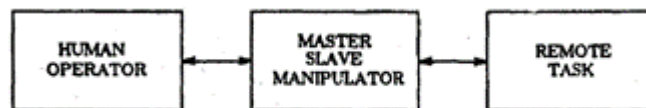


Figure 2.1: Model of master-slave system (13)

using a type of articulation for instance, a joystick. The corresponding forces are then transferred to the slave system in the direction as intended by the human operator and the remote task is accomplished. The goal of telerobot is essentially transporting a human operator in "sensation" to the remote location. This is also termed as *telepresence*. Sheridan also goes on to highlight that a telerobotic system must have complete *transparency*, which means that the end effector receives the forces as intended and transmitted by the human operator and the human operator receives useful information from the end effector about the forces experienced by the end effector due to its environment in the form of feedback.

2.2 CathBot

Based on the works of Kundrat *et al* (8), CathBot is a novel MR safe endovascular assisting robot platform. It is a telerobotic platform that is designed to enable endovascular procedures remotely. It consists of a primary system known as the master system and a secondary system or the slave system. The slave system is with the patient in the operating room. It is designed to be MR safe such that it could be positioned next to the patient during MR imaging. This is done to obtain position of the catheter. The master system is with the clinician/surgeon outside the operating room to reduce the surgeons exposure to radiation. At its current stage, the CathBot still employs X-ray fluroscopy to obtain the position of the catheter in the vasculature with ongoing testing to migrate the system to MR imaging in the future.

In its current form the master system consists of two motors which are responsible to provide haptic feedback to the user in the form of resistive forces offered by the motors against the motion of the user. The feedback mechanism in CathBot is also image based. It observes the catheter position within the vasculature. It defines a " σ " value which is a threshold value of the calculated distance between the catheter and the artery wall. If the distance is lower than the threshold " σ " value then it triggers the feedback system to provide haptic feedback to the user. Figure 1.2 shows the master and slave systems of CathBot.

2.3 Feedback

Feedback in a control system is a signal that is generated in response to the input signal provided to the system to offer corrective measures that can be applied to the input signal to reduce errors. For instance when applying a translation motion to an end-effector, the position feedback could be the difference between the desired destination point and the actual point of the end-effector. This feedback information can be then used to adjust the input signal to minimize the difference in desired and actual position of end-effector. Similarly in case of force feedback, the forces experienced by the end-effector can be transmitted to master system such that the input forces by the user can be adjusted. This feedback is especially useful when it comes to medical robotics since medical professionals require precision when conducting a medical procedure, absence of feedback especially in case of MIRS would limit the surgeons ability to manipulate the robot effectively and it would cause intra-operational damages to the patient thereby increasing the risk of injuries and therefore would result in a potentially negative safety implication.

Force feedback falls under the category of haptic feedback which is described as a feedback received by an user through the sense of touch, for instance the vibrations offered by a cellphone in response to a users typing can be considered as haptic feedback. It is essentially a mode of communication between an user and an electronic device or a robot. On an everyday basis humans integrate force and position feedback through mechanoreceptors, proprioception and vision (14). Since humans have so many sensory feedback systems in place, sensory integration and weighting takes place where weight of one sense is higher than the weight of the other sense and this is how humans fall prey to certain illusions. Based on the works of Mugge *et al* it can also be said that sensory weighting is guided by object stiffness and force feedback is weighted heavier with increasing object stiffness.

Haptic information provides important cues in teleoperated systems allowing the user to interact with the remote environment through the sense of vision and touch. The main objectives of designing haptic interface are stability and transparency. In case of medical robotics safety and reliability are also prime considerations(15). Some types of haptic technologies are:

- **Vibrotactile haptics:** Tiny motors that create vibrations in cellphones.
- **Microfluidics:** Air or liquid pushed in sockets of a smart textile to exert pressure or temperature on users skin.(16)

Kinaesthetic feedback: The feedback that provides the information of position and movement of a body especially received by proprioceptors.

Proprioceptors: These are nerve endings in nerves and joints that give information about the stretching and the movement of the muscles and joints.

2.4 Smart fluids

Smart fluids are fluids which have the ability to change their rheological properties under the influence of an external electrical or magnetic field. Some examples of smart fluids are electro-rheological fluids (ERFs), magnetorheological fluids (MRFs) and ferrofluids.

2.4.1 Electro-rheological Fluids (ERFs)

-rheological fluids (ERFs) are suspensions which have the ability to change their rheological properties reversibly under the influence of an external electric field (17). They can change from liquid-like material to solid-like material reversibly in milliseconds. This effect is termed as ER effect. ERFs consist of an electrically insulated liquid such as mineral oils with suspended fine particles of silica or starch which are of the magnitude of 50 micrometers. These particles are non-conductive but electrically active particles (18). It was reported that this fluid suspension increased its viscosity when exposed to an electric field.

2.4.2 Magnetorheological Fluids (MRFs)

Magnetorheological Fluids are smart fluids which have the ability to change their rheological properties under the influence of an external magnetic field. Ideally MRFs behave like a regular newtonian fluid when it is not exposed to any magnetic field. This also changes with the quantity of metal powder added to the fluid. When a magnetic field is applied, every metal particle becomes a magnet with north and south pole and it tends to form a link with the neighbouring particle. This chain link increases the viscosity of the MRF making it more "hard" (19).

MRF consists of 3 main components: The base fluid, metal particles and some additives.

The base fluid also known as the carrier fluid is composed of mineral oils, hydrocarbon oils or silicon oils. The fluid properties of the MRF are usually defined by the carrier fluid used and it also defines the thermal threshold for the MRF. Since temperature affects the viscosity of the oils it affects the overall viscosity of MRF as well.

Mixed in the oils are fine carbonyl iron or iron powder particles. They can constitute up to 50% by volume of the fluid. The particle size can be chosen based on the desired application. Usually the size of the particle ranges from 1-10 μ -meter. Larger particles will provide higher torque under magnetic field (19).

The additives are added to maintain the metal particles suspended in the carrier fluid. Usually if the fluid is kept for a long duration without action, the metal particles settle down and the fluid no longer displays MRF characteristics. To overcome this issue, additives are added to ensure that the metal powder remains suspended even if the fluid is in rest state for a long time. Usual additives are thixotropes, anti-corrosion components or highly viscous materials like grease (19).

2.4.3 Ferrofluid

Ferrofluid is categorized as a *colloidal suspension*. It consists of a carrier fluid and some suspended magnetic particles which are of the dimensions of ~ 10 nm (20). The magnetic particles are dispersed in the carrier fluid with varying magnetic moments such that the net magnetic moment of the fluid is zero (21). When this fluid is exposed to an external magnetic field, the magnetic moments of the particles align themselves along the magnetic field lines of the external magnetic field and give the aesthetic look of the ferrofluid as can be seen from figure 2.2. The key difference between the ferrofluid and MRF is the size of particles dispersed in the carrier fluid. The larger particles of MRF which are in the range of micrometers cause the fluid to be less stable than ferrofluid where the particles are small enough to remain suspended due to the brownian motion of the fluid. Table A.1 shows the data sheet of the ferrofluid employed in this thesis.

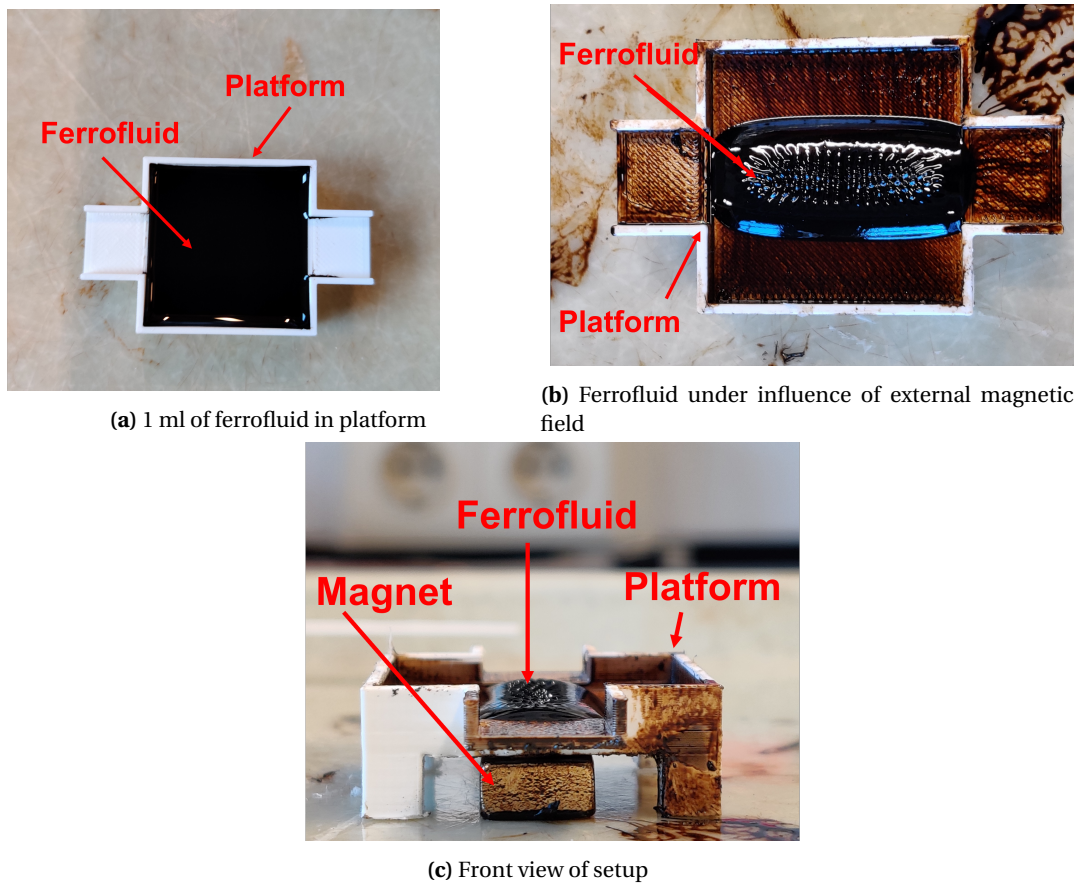


Figure 2.2: Volumetric redistribution of ferrofluid under the influence of an external magnetic field

3 Design

In this chapter, the concept design which is envisioned for a ferrofluid based feedback system for the master system of CathBot is discussed. The requirements for a 3-D tactile feedback are discussed and key assumptions regarding the ferrofluid behaviour were made in the design phase. The design of the experimental setups along with the design for the models are also discussed in this chapter.

3.1 Concept envisioned for ferrofluid based feedback system

In order to provide a tactile feedback to a user of the CathBot, a mechanism should be developed through which a user would essentially have the same "feeling" as the user would have when actually manipulating a catheter/guidewire. To enable this, a system should hence have the ability to transfer the forces experienced by the catheter at the slave end of the CathBot to the master side such that the user experiences those forces and also has information about which point on the catheter has made an contact with the artery wall such that the user is able to manipulate the catheter quickly and intuitively, away from the contact point.

An initial design approach was a top down approach that involved a design concept for an enclosed case that would mimic a vasculature. Four base directions "UP", "DOWN", "LEFT", AND "RIGHT" were considered for the optimum directional feedback to be provided for the user. Hence a square case was imagined. Internal flaps present inside the square case capable of deflections of 5 mm or more at forces as low as 0.0098 Newtons were envisioned. A plunger which would be gripped by the user was also designed attached to the user handle of the master system of the CathBot as can be seen figure 3.3. The plunger would ideally bend in the direction a catheter/guidewire would bend in the vasculature on the slave side thereby providing a tactile feedback to the user gripping the plunger. The deflection in the flap would provide forces for the plunger to bend in a certain direction. The deflection was assumed to be achievable by the action of ferrofluid present between the region of the flap and the case. Figure 3.1 shows the cross-sectional view of the case. The region marked in red are the four flaps which would deflect for their corresponding direction. The region in gray colour is an empty space which would be filled with ferrofluid

Ferrofluid is assumed to produce the necessary forces for the deflection in the flap of the model under the influence of an external magnetic field. The mouth of the case is to be sealed with a flexible latex based seal such that it does not allow ferrofluid to leak out of the case and also does not provide any additional forces to the plungers or the deflecting flaps. To keep the region inside the case free of air a vacuum chamber was designed. The chamber is used as a filling point from where ferrofluid is added to the case until the entire case is completely filled with ferrofluid. The vacuum chamber is then closed and sealed to create a negative pressure if fluid would were to start to flow inwards the case. Figure 3.3 shows the model with vacuum chamber.

3.2 Design of Validation experiments

To validate the design assumption that ferrofluid is able to deflect the flap in figure 3.1 under the influence of an external magnetic field, two experiments were designed:

- Flap elevation test
- Weight experiment

The Flap elevation test was designed to validate if ferrofluid under the influence of an external magnetic field is able to elevate a flap. To achieve this an isolated flap based on the flap in the

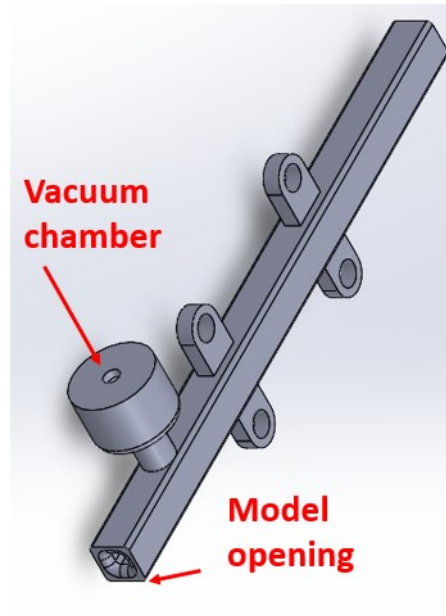
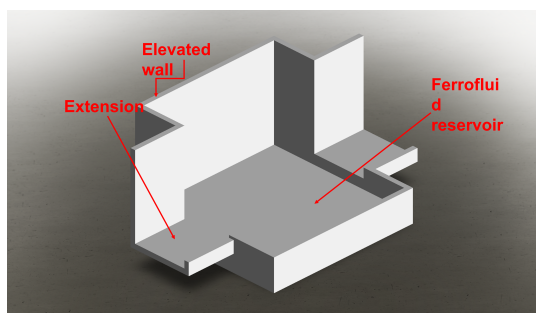
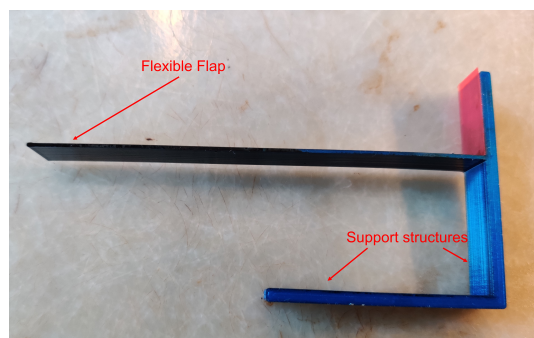


Figure 3.3: Envisioned ferrofluid case



(a) 3-D printed platform (White Tough PLA)



(b) 3-D printed flap (Blue PLA)

Figure 3.4: Examples of platform and flap

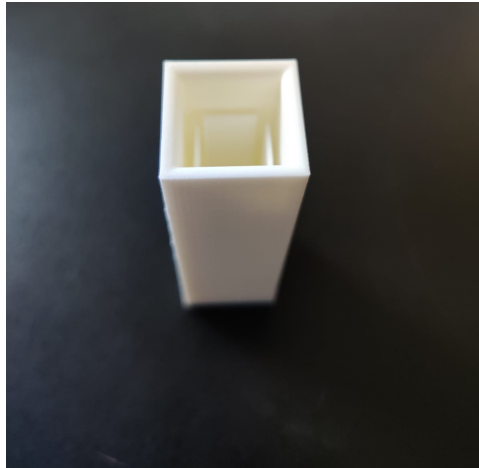


Figure 3.5: 3-D printed Model-1 design

figure 3.1 was designed with a thickness of 0.5 mm, a length of 90 mm and a width of 10 mm. Additional support structures were also provided to the flap such that the flaps bottom surface is at an height of 28 mm from the surface it is kept on as seen in figure 3.4b.

A platform also was designed such that it could accommodate 1 mm - 2 mm thick film of ferrofluid on its flat surface. The flat surface of the platform as highlighted in figure 3.4a was surrounded with a wall to retain the ferrofluid. Leg extensions were designed to elevate the platform to accommodate an electromagnet/permanent magnet under the platform. Platform extensions were additionally designed to support the flap discussed above on these extensions. The height difference between the extension surface and the flat surface is 1 mm. This was done to provide space for ferrofluid to be under the flap, and to prevent any buoyancy forces that may occur if the flap was directly submerged in the ferrofluid.

3.3 Model design

The design for the model was based on the concept design. The model was 3-D printed using White Tough Polylactic Acid (PLA) with a outer case thickness of 2 mm. The flaps were with a thickness of 0.5 mm and the internal distance between the flap was 12 mm. The height of the model designed was kept at 60 mm to mimic half the travel distance of the user handle of CathBot. The height of flaps were kept at 45 mm to provide leeway between the case opening and flap free end for potential sealing strategies. Figure 3.5 shows the model-1.

Two additional variations were also designed and manufactured based on model-1. Model-2 was made identical to model-1 in design but the composition of the flaps were changed. The inner flaps of model-2 were made of thermoplastic polyurethane (TPU95A) for additional flexible advantage. Model-3 was designed to be cylindrical, with a cylindrical inner flap made of TPU95A. The cylindrical design was done to mimic the typical shape of an artery. The outer case of model-3 was made of white tough PLA. Section 4.2.2 discusses more about these variations.

3.4 Plunger

The requirement for the plunger was that it could facilitate bending at forces lower than 0.0098 N and yet maintain its rigidity and not bend due to the effect of gravity or self weight. The length of the plunger was designed with 100 mm length with width and height being 2.5 mm each. Figure 3.6 shows the designed plunger. An additional design at the plunger head was designed for the user study experiment to facilitate the connection between the plunger and the aluminum assembly which is explained in section 4.4. The plunger was 3-d printed using Ultimaker S5 3-D printer. The material used for the plunger was TPU95A, a 3-d printer filament that produces



Figure 3.6: Plunger

flexible 3-D prints with high elasticity.. It is ideal for materials to be 3-D printed with rubber or plastic-like properties.

The design for the plunger was inspired by the catheter but with a square profile for the user to grip.

The use of the plunger as envisioned with the concept design is such that the user would grip the user handle of the CathBot with index finger, middle finger and thumb and simultaneously grip the plunger with ring and little finger. This way the force feedback by the brushless DC motor is received along with the knowledge of the directional forces is received from the ferrofluid based feedback system.

4 Experimental Setup

4.1 Validation and evaluation Experiments

To validate the design concept a set of experiments were performed to test the design assumptions. The Flap elevation test describes the procedure employed to prove that ferrofluid under the influence of external magnetic field is able to elevate a 90x10x0.5 mm flap made of Polyactic Acid (PLA) as shown in figure 3.4b. The flap elevation test was first conducted with an electromagnet and then with two permanent magnets as described below.

The force exerted by the ferrofluid was evaluated through a flap-platform based setup. The optimum position of the electromagnet on the model was also estimated with a model test. The section is concluded with the description of an user study which provided some insights into the feasibility of the model.

4.1.1 Flap Elevation test

This test was conducted to validate the design assumption that ferrofluid is able to accumulate itself along the external magnetic field lines such that it is able to cause a visible elevation in a 90x10x0.5 mm flap made of PLA in the range of 0.5-1 mm as explained in section 3.2. The experiment was conducted with an electromagnet and then carried over by permanent magnets of higher magnetic field strength.

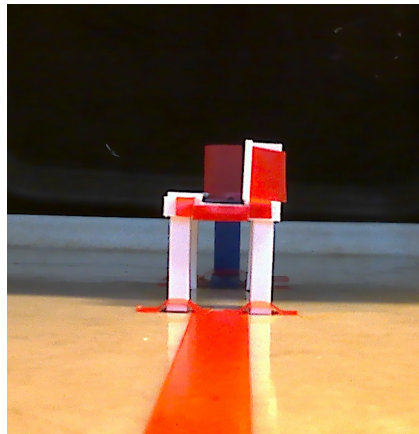
With Electromagnet

The first assumption was that the viscosity of fluid would change under the influence of an external magnetic field which would potentially result in the expansion of the fluid causing it to bend the flap and the second assumption was that an oleophobic coating, due to its oil repelling properties may improve elevation in the flap. To test these assumptions a setup was designed consisting of a 3-D printed platform made of white tough PLA and two identical flaps made of blue PLA as seen in figure 3.4. One of the two flaps was coated in an oleophobic coating. The flaps were designed to be as thin as possible so that they are flexible such that a force of 0.005 N applied at the free end of the flap could cause the flap to bend. In this case the flap thickness was 0.5 mm.

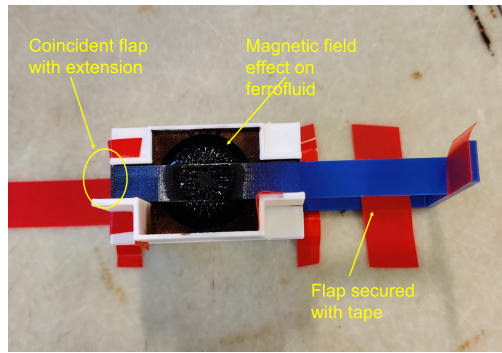
The setup required that the platform and one of the flaps to be positioned such that the flap rested just above the platform as can be seen in figure 4.1b. A LAMAX X7.1 NAOS action camera A.3 was used to capture images. Figure 4.1a shows an image acquired from this camera. The camera was positioned with respect to the flap setup to capture the images of the flap at different instances during the experiment as seen in figure 4.1c. The camera was placed at a distance of 21 cm from the edge of the platform. It was discovered through iterative optimization of image acquisition that the images acquired at this distance were in focus and optimum to perform edge detection after image acquisition as described in section 4.3. Care was taken such that the flap coincided with the edge of the platform when seen from the top as shown in figure 4.1b, to ensure that the image acquired from the camera captures the flap end as well as the edges of the platform in the same plane, to help with estimating the relationship between number of pixels and length as explained further in section 4.3.

This experiment was conducted using an INTERTEC ITS-MSM-1515-12VDC, 1.4W electromagnet with a maximum holding force of approximately 2.04 kg, and was positioned under the platform initially. The electromagnet when activated would act as a source for an external magnetic field for the ferrofluid.

The experiment was performed with a non-coated flap followed by the oleophobic coated flap. The process of the experiment is as depicted in 4.2a. The initial image of the setup as described above was captured. Approximately 0.5-1 ml of ferrofluid was added to the flat portion



(a) Front view of the flap elevation test

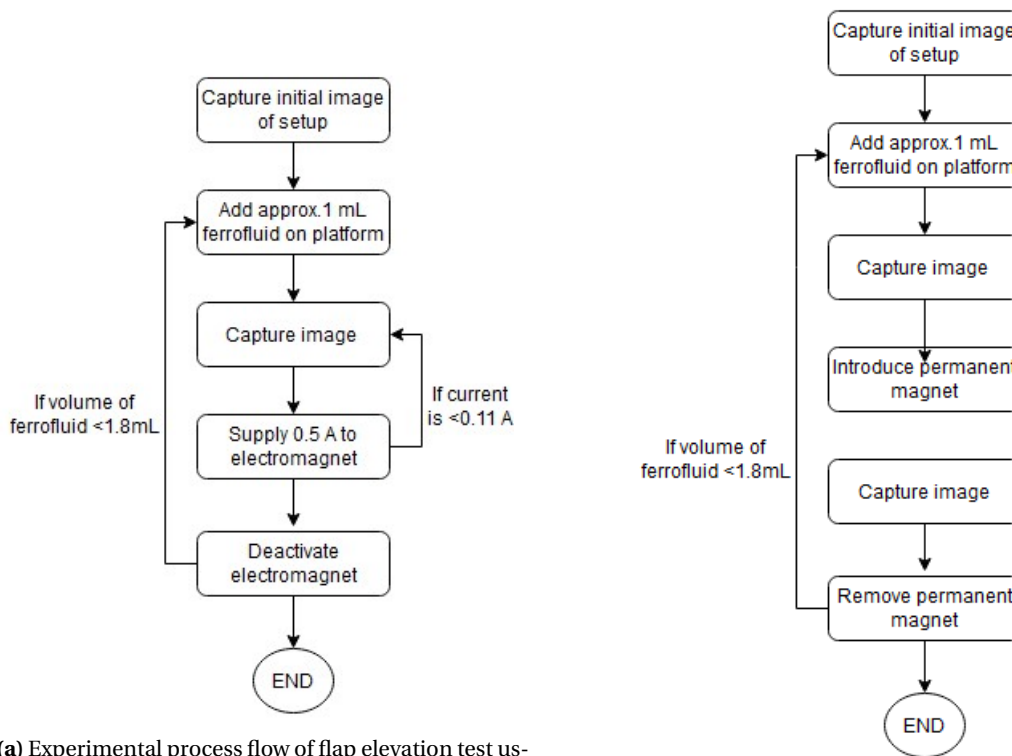


(b) Flap-platform coinciding at extension and ferrofluid under the influence of an external magnetic field



(c) Top view of the flap elevation test

Figure 4.1: Experimental setup for the flap elevation test. Red tape was used to mark and secure flap and platform positions



(a) Experimental process flow of flap elevation test using electromagnet

(b) Experimental process flow of flap elevation test using Permanent magnet

Figure 4.2: Experimental process flow for flap elevation test

of the platform using a syringe. The purpose for using approximately 0.5-1 ml of ferrofluid was to create a 1 mm thick layer of ferrofluid on top of the flat surface of the platform which had a flat surface of $29 \times 29 \text{ mm}^2$. Another image was captured and the electromagnet was activated and an initial current of 0.05 A was applied. An image was captured of the setup in the powered ON state. An increment of 0.05 A was given to the electromagnet and yet again an image was captured. This process was repeated thrice until a maximum current of 0.11 A was reached at 13.6 V. The electromagnet was deactivated at this stage. The volume of the ferrofluid in the platform was doubled to obtain higher values of elevation due to increase in volume of ferrofluid and the experiment was repeated again. After maximum current was reached a second time, the electromagnet was deactivated and the experiment was concluded. The non-coated flap was then replaced with the coated flap and the entire process was repeated. A total of 8 images of the non-coated flap and 8 images of the coated flap setup at different instances of current and voltage are acquired. The acquired images are then processed as explained in section 4.3 and the results are tabulated in the results section.

With Permanent Magnet

The purpose of using permanent magnets instead of the electromagnet was to observe if increase in the magnetic field strength had any impact on the action of the ferrofluid. The permanent magnets were also dimensionally smaller compared to the corresponding electromagnets of similar strengths. The setup used in 4.1.1 which was conducted with the electromagnet was replicated for this experiment with a few changes. Alterations were made to the platform, namely a sump was added at the extensions to prevent the ferrofluid from leaking from the platform. Figure 4.1c shows the top view of the setup with the new platform. Figure A.2 shows the two different platforms. Two permanent magnets, a countersunk N35 Nickel plated disc magnet CS-S-18-04-N with a holding force of approximately 4kg and a Neodymium N42 disc magnet S-20-08-N with a holding force of approximately 9.3 kg were used in succession to evaluate elevation as described in 4.1.1. The setup was also secured to the base such that the platform or the flap would not displace when the magnet was introduced underneath the platform. Figure 4.2b shows the process flow followed with the permanent magnets.

Initial experiment was conducted with the countersunk CS-S-18-04-N magnet and was then followed by with S-20-08-N magnet. An initial image of the setup was captured before adding approximately 0.5-1 ml of ferrofluid on the platform. Another image was then captured and a permanent magnet was slowly introduced underneath the platform using a 3-D printed magnet case as seen in A.4. To avoid sudden impact that the magnet causes due to the attractive force between the magnet and the ferrofluid the magnet is slid into position from the direction where the platform has an elevated wall using the magnet case to ensure that no ferrofluid escapes from the platform. The magnet was positioned directly under the platform at the center below the flap as can be seen in figure 4.1b. Another image of the setup is captured in this state. The magnet is then removed and the initial volume of the ferrofluid added to the platform is doubled to estimate effect on elevation for increased volume of ferrofluid. The process is repeated. A total of 5 images of the experiment per magnet were captured.

4.1.2 Evaluation of force exerted by ferrofluid

The following experiment was conducted to evaluate the force that the ferrofluid is able to exert on the flap shown in figure 3.4b. The experiment setup as described in the flap elevation test with the permanent magnet was replicated for this experiment. The ring magnet and the disc magnet described above were also used. The purpose of using these magnets was to evaluate if the strength of a magnet affected the ferrofluids ability to exert force. Non-magnetic standard brass weights were used in this experiment. Figure A.1 shows the weights. Figure 4.3 shows the process flow of the experiment.

The platform and the flap are arranged as explained in section 4.1.1 and an image of this ini-

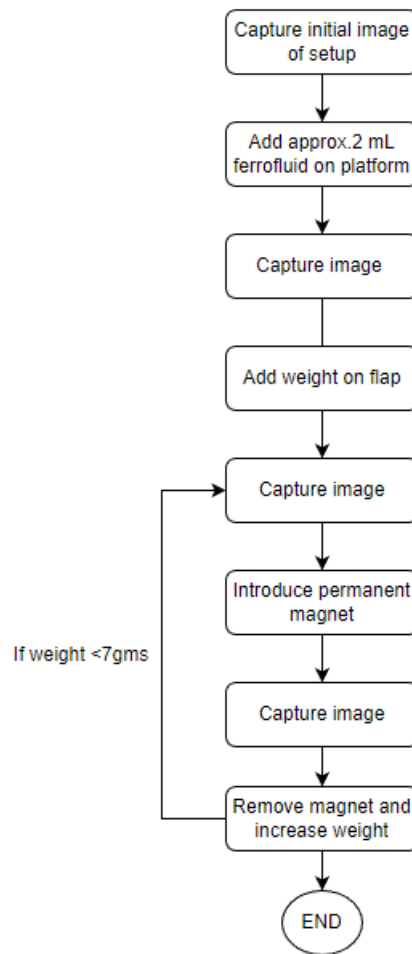


Figure 4.3: Experimental process for evaluating force exerted by ferrofluid

tial condition was captured as reference. Another image after adding approximately 2 ml of ferrofluid on the flat surface of platform was captured. A standard non-magnetic brass based weight of 1 g was placed on the flap at a distance of 80mm from the fixed edge of the flap. An image of the setup at this stage was captured. The permanent magnet was then introduced in the same manner as explained in the previous section. An image of the setup was acquired again with the magnet. Weight on the flap was then incremented by 1 g and the process was repeated until there was no observable movement in the flap. The concept of balancing two torques was used to design this experiment. Figure 4.4 shows a schematic diagram of the forces experienced by the flap. The torque offered by the known weight is the self weight multiplied with the distance from the fixed edge. The ferrofluid also exerts a force "X" as depicted in the diagram. The known weight is added until no visible elevation is observed in the flap. The images acquired are then processed. The results are tabulated in the result section. The calculation of forces is further explained in section 5.2.

4.2 Model testing

Concluding the validation experiments were critical to estimate if the feasibility of the concept. From the flap elevation test and the evaluation of force exerted by the ferrofluid I could conclude that the ferrofluid under an external magnetic field is able to exert a force on the flap as you will see in chapter 5. It was then decided to design a model to determine an optimum position for a magnet keeping the envisioned concept of the feedback system as explained in section 3.1 in mind. The model named as *model-1* as shown in figure 4.6 was hence designed

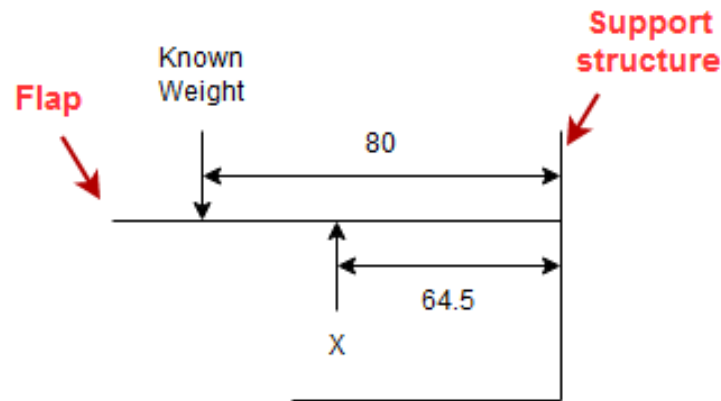


Figure 4.4: Schematic representation of forces experienced by a flap

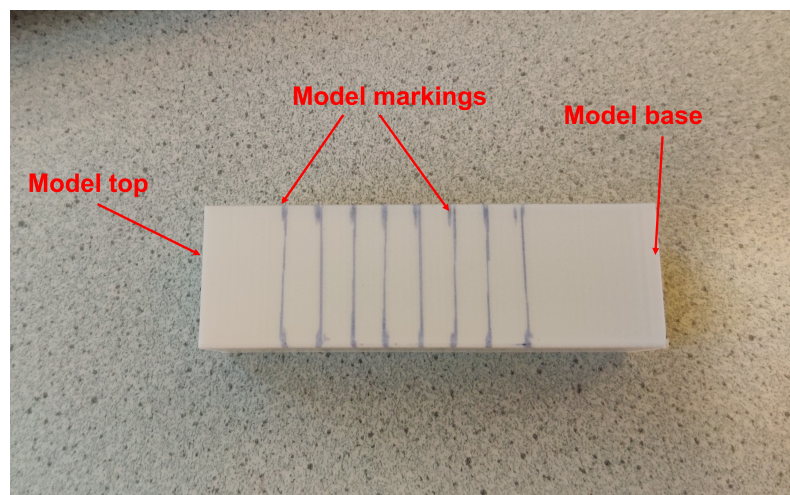


Figure 4.5: Reference markings for magnet position on outer surface of model-1

and 3-D printed using white tough PLA to evaluate the optimum position for the magnet to be placed. The minimum distance between the magnet and the outer surface of the model required for the magnet to influence the ferrofluid inside the model for a deflection higher than 1 mm of the flap was also evaluated using three variations of model-1 as explained in section 4.2.2.

4.2.1 Experiment-1: Evaluation of optimum position for magnet on model surface

This experiment was designed to estimate the required position of the magnet on the surface of a model containing ferrofluid for a maximum observable deflection. Model-1 as can be seen in figure 4.6 was clamped in position. The external surface of the model were marked as reference positions for the magnet as shown in figure 4.5. Three Neodymium N42 disc magnets, S-20-08-N (Magnet 1) with a holding force of approximately 9.3 kg, S-20-15-N (Magnet 2) with a holding force of approximately 13 kg and S-20-20-N (Magnet 3) with a holding force of approximately 15 kg were used in succession for this experiment. Since the diameter of all three magnets is 20 mm, the markings on the case were also done at an offset of 20 mm from the base of the model with an increment of 5 mm until the 55 mm mark from the base of the model.

A oneplus 7 phone camera was positioned such that the top-view of the model is visible as can be seen in figure 4.6. An initial image of the setup was captured and 10 ml of ferrofluid was added to the model. Another image was captured after adding the ferrofluid. The S-20-08-N magnet was positioned at the base of the model as can be seen in figure 4.6 and an image of

the same is captured. The magnet is moved upwards with an increment of 5 mm and another image was captured. This process was repeated until the edge of the magnet reached a height of 45 mm such that the center of the magnet is at a distance of 35 mm from the base of model-1. the magnet is then replaced with S-20-15-N and the whole process is repeated until all 3 magnets described above are used to perform the experiment. The images acquired are then processed and the results are tabulated in the results section.

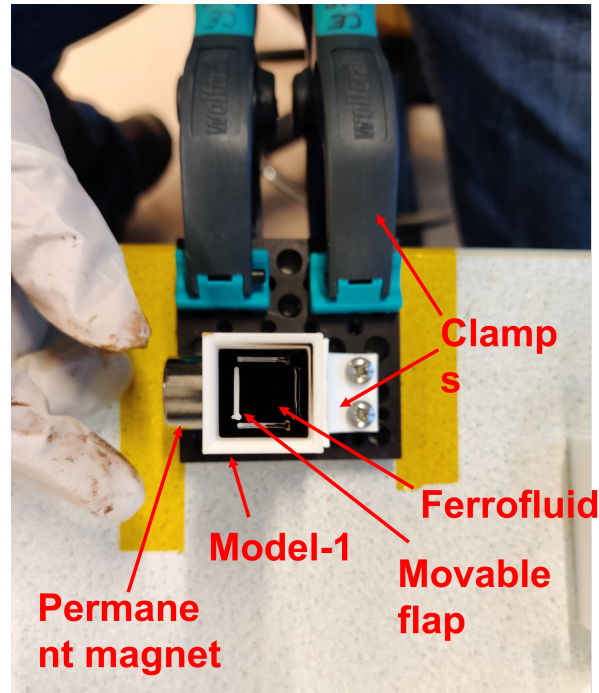


Figure 4.6: Top view of model-1 with permanent magnet positioned on external surface of model

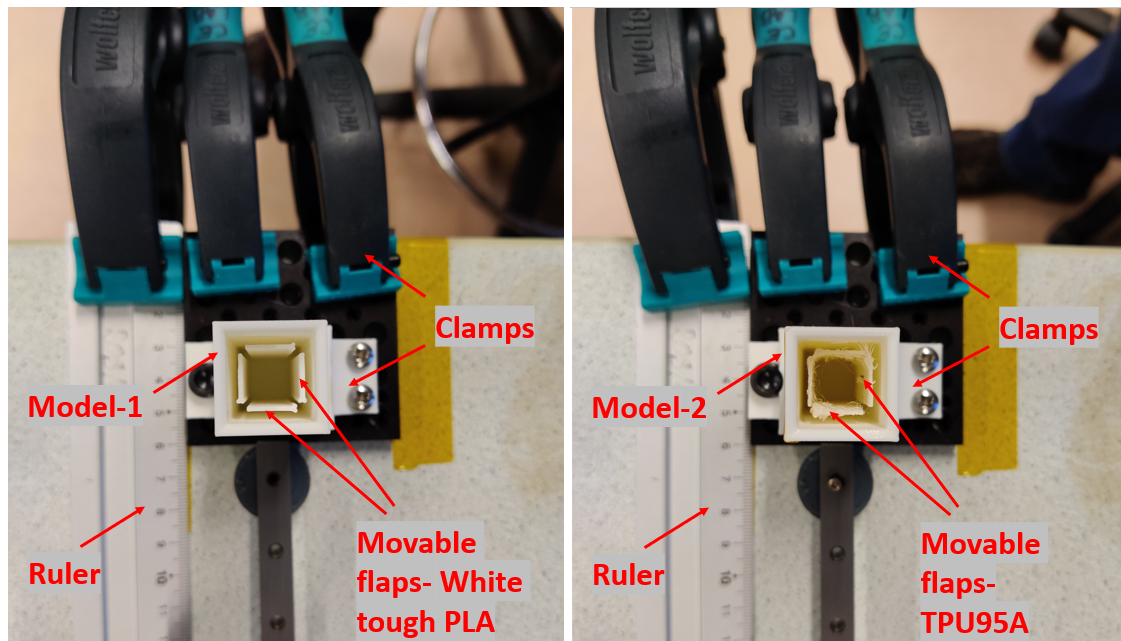
4.2.2 Experiment-2: Evaluation of optimum distance between magnet and model surface for deflection in flap

This experiment was designed and conducted to evaluate the minimum distance required between the magnet and the outer surface of a model containing ferrofluid for a deflection of flap to occur. Two additional variations of model-1 were designed as can be seen in figure 4.7.

1. *Model-1* : Composed entirely of white tough PLA
2. *Model-2* : Outer case composed of white tough PLA, Inner flaps TPU95A
3. *Model-3* : Cylindrical outer case composed of white tough PLA, Inner cylinder TPU95A.

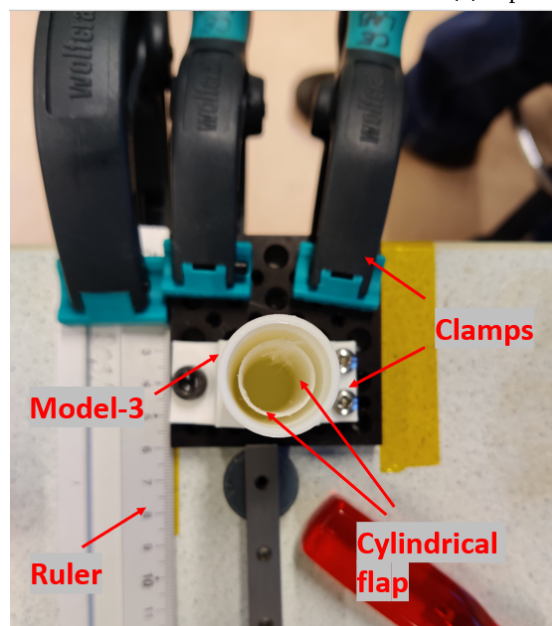
The three models were designed to evaluate the action of the ferrofluid under the influence of different levels of magnetic field strength at different distances. The inner flaps were also composed of different materials as listed above. Model-3 was also designed with a circular cross-section. The circular cross-section was chosen as it mimics the cross section of a typical blood vessel.

For this experiment *model-1* was clamped into position in a vertical orientation such that the model opening could be seen from the top view. Figure 4.8 shows the experimental setup. An image from the top view of the model was then captured. Figure 4.7a shows the top view of model-1. 10 ml of ferrofluid was added in to the model. A magnet holder A.5 was mounted on a movable tray for the magnet which would move perpendicular to the surface of model-1. A ruler was placed next to movable tray to estimate the distance of the magnet from model-1. A



(a) Top view of model-1

(b) Top view of model-2



(c) Top view of model-3

Figure 4.7: Top view three different model variations

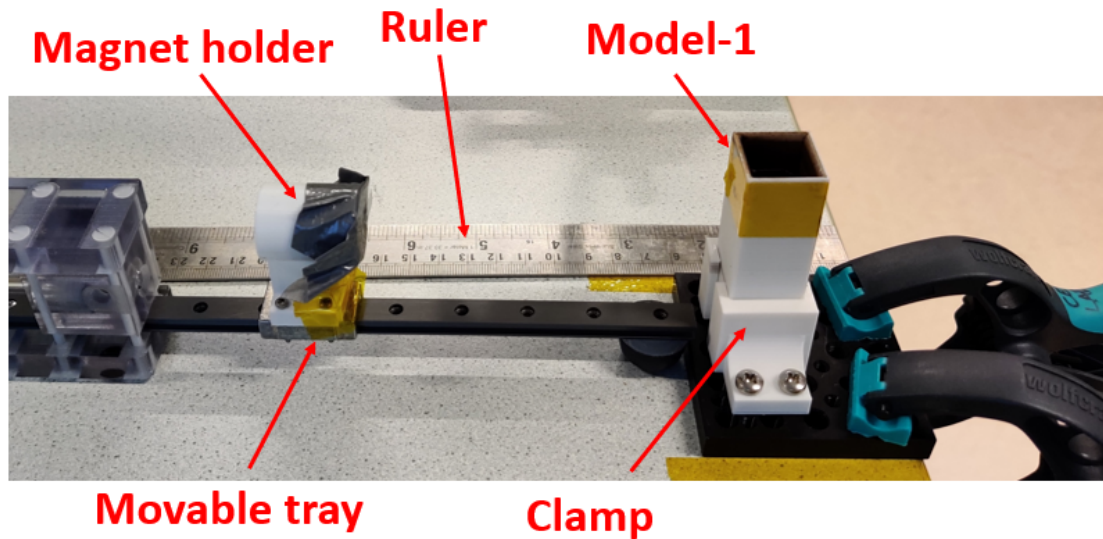


Figure 4.8: Experimental setup with movable magnet

one plus 7 phone camera was used to acquire the images from the top view to record deflections of the flap at different distances of the magnet from the model. To begin the experiment an image of the model with the ferrofluid was captured to note the initial position of the flaps. The S-20-08-N permanent magnet was positioned at a distance of 7 cm from the outer surface of *model-1*. Another image was captured and the distance between the magnet and the outer surface of *model-1* was reduced by a factor of 1 cm. This process was repeated until the magnet was in contact with the outer surface of *model-1*. When the distance between the magnet and the model was 1 cm, the reduction factor was changed to 0.5 cm.

Three Neodymium N42 disc magnets, S-20-08-N with a holding force of approximately 9.3 kg, S-20-15-N with a holding force of approximately 13 kg and S-20-20-N with a holding force of approximately 15 kg were used in succession for this experiment. This experiment was then repeated for model 2 and model 3 with all three magnets. The acquired images were then processed and the results discussed in the result section.

4.3 Image Processing

The images acquired from the validation and evaluation experiment and images of model-3 from model test are processed differently from the images acquired from the model tests with the exception of model-3 since the camera acquiring the images in the two cases were different. The errors occurring due to camera distortion are neglected in this assignment.

The acquired images from the validation and evaluation experiments and images of model-3 are processed through a MATLAB script A. The script initially reads a RGB image obtained from the camera. It then converts the RGB image into a gray-scale image and applies a *canny* edge detector (22). The function *impixelinfo* is used to obtain the pixel data. The output image provides pixel information namely the *x* and *y* coordinates of the pixel highlighted by the cursor. Using the pixel coordinates of the final image as shown in figure 4.9d, the linear distance between the flap and the platform is calculated at three different points namely: Left extreme (L), right extreme (R) and central point (C) of the flap as shown in figure 4.9d. An average of the three obtained values is computed and the result is then tabulated in the results section. The number of pixels that constitute distance between the platform extension edges as shown in figure 4.9d is also obtained. This number gives the thickness of the platform extension in number of pixels. It is used to derive a relationship between the number of pixel and the known thickness of the flap in the results section.

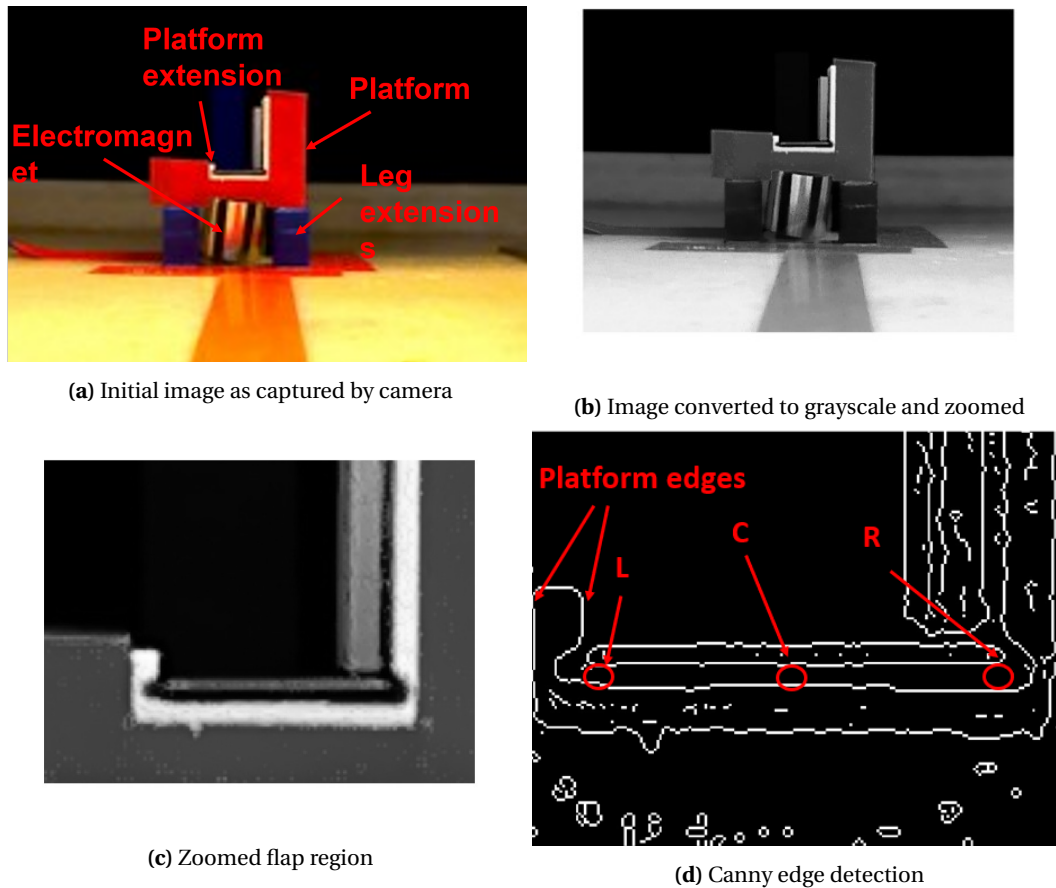


Figure 4.9: Image processing process for images acquired from validation and evaluation experiments

The acquired images from the model tests were initially cropped to show only the top-view of the model face. The cropped images were then processed through a MATLAB script A with the exception of the images of model-3. The cropped images are rotated anti-clockwise by an angle of 33° . The image is then converted to gray-scale. A canny edge detector is then applied to the gray-scale image. the coordinates of the line segments in the detected edges are then obtained using hough transform (22). The detected line segments are then overlaid on the original image as shown in as shown in figure 4.10. The detected line segment of the flap and the inner case of the model are assumed to be parallel.

The line coordinates corresponding to the flap and the inner edge of the model are then processed through another MATLAB code A to obtain the distance between two parallel lines. The results obtained are then discussed in the results section. The thickness of the flap in pixel is also obtained by measuring the distance between two parallel line segments detected by hough transform which correspond to the lines of the flap highlighted as flap lines in figure 4.10. This gives the relationship between pixel and mm for conversion as can be seen in the result section.

4.4 User Study

A user study with 10 volunteers composed of 9 university of students and a researcher was conducted to access if the deflection provided by the flaps due to the action of an external magnetic field on ferrofluid within model-1 was sufficient to deflect a 3-D printed flexible 2.5X2.5X100 mm *plunger* made of TPU95A, such that a user is able to acknowledge the bending of the plunger and the direction of bending of the plunger through tactile senses. Figure 4.11 shows the setup used for the user study. The setup is aligned in a horizontal setting due to the absence

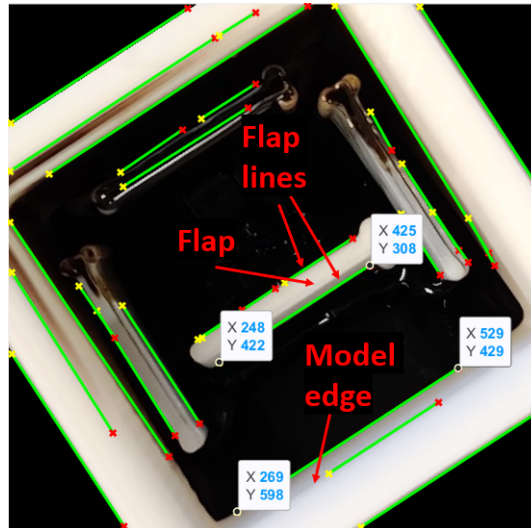


Figure 4.10: Overlay of hough lines on cropped image of top view of model-1 with a deflected flap

of adequate sealing of the face of model-1 for the ferrofluid present within model-1. The study focused on three cases, namely:

1. Position on the plunger
2. Holding style
3. Visual perception

4.4.1 Position on the plunger

The plunger was marked at two positions for the users to hold at, 10mm and 30mm respectively as measured from the face of the model as explained in setup in figure 4.12. The purpose of two positions on the plunger was to evaluate if users were able to acknowledge the plunger bending and direction of bending at different distances from the face of model-1.

4.4.2 Holding style

Two different holding styles were demonstrated to the users to hold the plunger for this study. The first holding style was using index finger and thumb with a relaxed grip as a user would hold a pen or a pencil between the thumb and index finger as shown in figure 4.13a. The second holding style demonstrated was using the ring and the little finger and holding the plunger as shown in figure 4.13b.

The first holding style is intuitive to users. The purpose for the first holding style was to evaluate if users were able to perceive movement and the direction of the movement occurring in the plunger using an intuitive holding style. The purpose for the second holding style was due to the fact that the final use case of the feedback system as envisioned would require the user to grip the *user handle* as described in the works of Kundrat *et al* (8) with the index finger, middle finger and thumb while the ring and little finger would hold the plunger as described above to receive tactile feedback.

4.4.3 Visual perception

The works of Brodoehl *et al* (23) suggests that the fingers becomes more sensitive when users close eyes in darkness. It is also proven in a study conducted by Goldreich *et al* (24) that tactile acuity is enhanced in blindness. Hence absence of visual perception has an effect on tactile sensitivity. The two variations in the study are hence the presence (eyes open) and absence

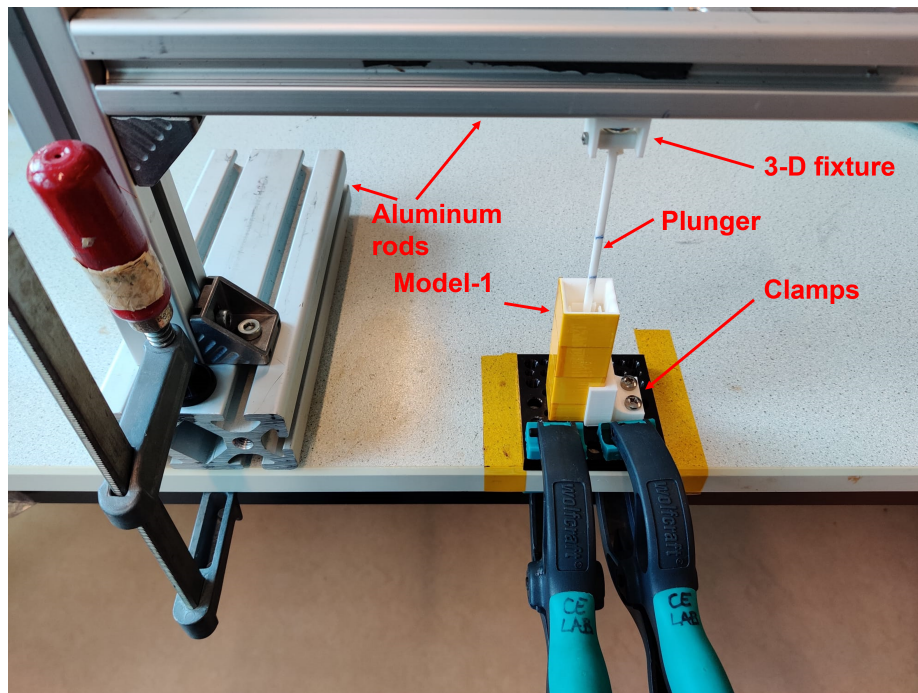


Figure 4.11: Setup with aluminum rods for User study

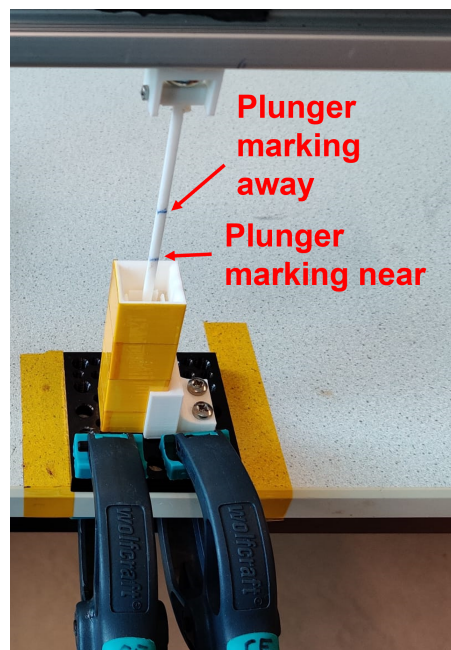
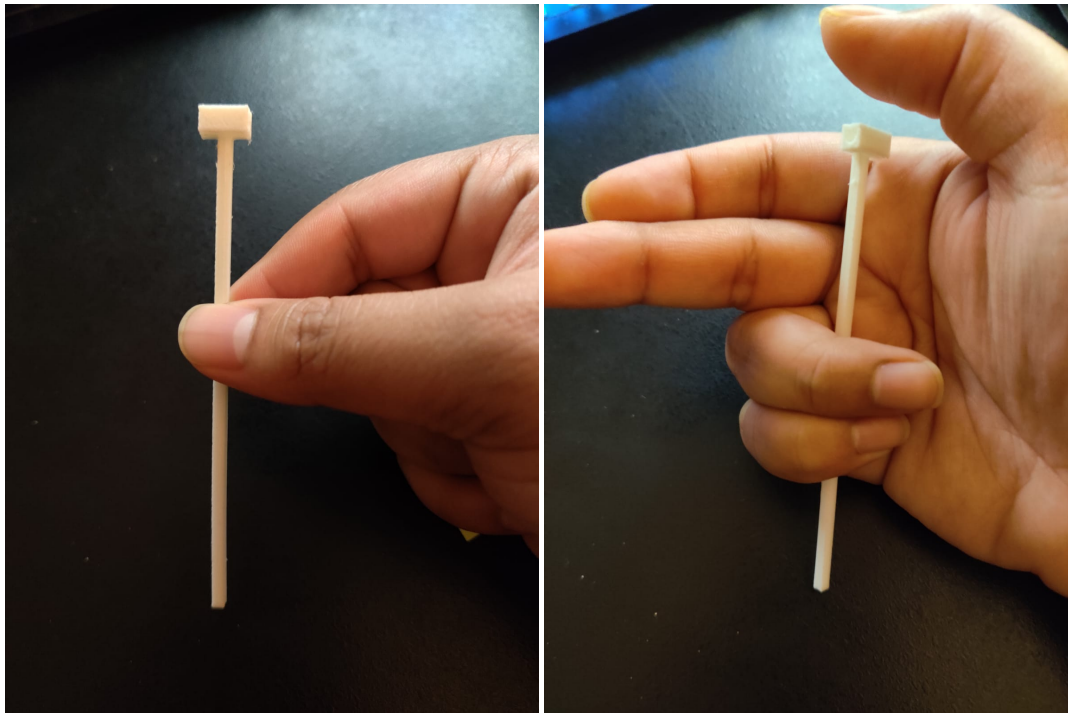


Figure 4.12: Markings on plunger away and near from the face of model-1



(a) Holding plunger with index finger and thumb (b) Holding plunger with ring finger and little finger

Figure 4.13: Different holding styles of plunger

(eyes closed) of visual perception in the users.

The user study involved recording haptic perception of the user in eight different variations as explained below:

1. Index finger and Thumb Closed Eyes Near model (**ITCN**)
2. Index finger and Thumb Open Eyes Near model (**ITON**)
3. Ring and Little finger Closed Eyes Near model (**RLCN**)
4. Ring and Little finger Open Eyes Near model (**RLON**)
5. Index finger and Thumb Closed Eyes Away model (**ITCN**)
6. Index finger and Thumb Open Eyes Away model (**ITON**)
7. Ring and Little finger Closed Eyes Away model (**ITCN**)
8. Ring and Little finger Open Eyes Away model (**ITON**)

Five readings were recorded for every variation. The experimental setup consisted of aluminum rods setup as can be seen in figure 4.11. The model was clamped to restrict movement and the plunger was fixed at one end with 3-D printed fixtures to the aluminum rod and freely suspended such that it was positioned in the center of the model-1. The model was filled with 10 ml of ferrofluid.

The volunteers for the study after signing a consent form were then given a brief explanation of the different variations listed above and were directed to have a relaxed hold on the plunger at two different points marked on the plunger. The two different holding styles were also demonstrated to the volunteers. they were also advised to position the plunger centrally aligned to the center of the model-1 as much as possible. The volunteers were further instructed to not look at the setup when the eyes were to be kept open. The volunteers were also advised to be aligned

directly facing the setup such that their body is parallel to the setup plane. No additional information was provided to the volunteers so as to avoid any bias based feedback.

During the experiment a permanent magnet S-20-20-N was used as a source of magnetic field for the ferrofluid within model-1. The order in which the variations were tested out were randomized for every volunteer. The direction of the magnet introduced to model-1 was also randomized. After all the above listed variations were completed the volunteers were asked to fill out a brief questionnaire and the study was concluded. The results obtained were then tabulated and are then discussed in the results and discussion sections.

5 Results

In this section the results of flap elevation test, evaluation of force exerted by ferrofluid, model test experiments and the user study are tabulated and the observations based on the tables are discussed for every experiment. The flap elevation tests provides evidence for the feasibility of the concept. The amount of force exerted by the ferrofluid on the flap is calculated using balancing of torques. The model test provides an optimum position for a magnet to be placed, it also shows the distance a magnet must be to have an impact on the ferrofluid within the model. The user study provides interesting insights on accuracy of the feedback system in a horizontal configuration.

5.1 Flap elevation test

The results obtained from the image processing of flap elevation experiment were tabulated giving details about the average elevation of the flaps at different instances of current as well as different magnetic field strengths. The conversion from pixel to mm is also calculated in this section.

5.1.1 With Electromagnet

The initial observation made while conducting the flap elevation experiment with an electromagnet was that the flap was already elevated after adding the ferrofluid to the flat surface of the platform. There was no additional elevation observed visually when the electromagnet was activated. Table 5.1 shows the amount of elevation in non-coated flap at different instances of current and voltage supplied to the electromagnet when the volume of the ferrofluid is in the range of 0.5-1 ml. It can be observed from table 5.1 that the difference between the flaps initial position when supplied voltage is 0 V and the flaps position at the maximum power supplied to the electromagnet at 13.6 V is

$$7.67 - 7 = 0.17 \text{ pixels}$$

To convert pixels into mm the thickness of the extension edge is taken as control as shown in

Table 5.1: 0.5-1 ml non-coated flap elevation at four instances of current

Voltage (V)	Current (A)	Average Elevation (pixel)	Average Elevation (mm)
0	0	7.5	0.40
5.8	0.05	8	0.42
11.5	0.1	7.67	0.41
13.6	0.11	7.67	0.41

figure 4.9d. Since the dimension of the edge is known and it lies in the same plane as the flap, it was used to convert number of pixels to mm for this experiment. In this case the dimension of the edge was 1 mm which translates to 19 pixels in the image taken.

Therefore,

$$\begin{aligned}
 19 \text{ pixels} &= 1 \text{ mm} \\
 1 \text{ pixel} &= 0.053 \text{ mm}
 \end{aligned}
 \tag{5.1}$$

The values in table 5.1 for average elevation are depicted in pixels and converted to mm using the relationship in equation 5.1. The values of mm are rounded off to 2 decimal places as the

resolution of data in this document is maintained at 2 decimal places as explained in A.1 . From table 5.1 we can see that the elevation in the flap is 2.5% (0.01 mm) higher at 13.6 V (maximum power) compared to the initial condition at 0 V (initial condition).

Table 5.2 shows the amount of elevation in a flap coated with an oleophobic coating at different instances of current and voltage supplied to the electromagnet. As can be observed from the table values, there is no change in the average elevation values of the flap between the initial condition at 0 V and the final condition at 13.6 V, where maximum power (beyond the rated value of 1.4W) was supplied to the electromagnet.

The ideal flap elevation which is useful for the concept as explained in A.1 is 0.5-2.67 mm for

Table 5.2: 0.5-1 ml coated flap elevation at four instances of current

Voltage (V)	Current (A)	Average Elevation (pixel)	Average Elevation (mm)
0	0	6.67	0.35
5.8	0.05	7	0.37
11.1	0.1	6.67	0.35
13.6	0.11	6.67	0.35

0.5-1ml of ferrofluid. In both the tables the elevation observed is lesser than required for the purpose of this thesis and hence the volume of the ferrofluid was doubled to approximately 1.8 ml and the experiment was repeated and the results were tabulated in 5.3 and 5.4

As we can observe from table 5.3 the elevation in the flap is 7.7% (0.03 mm) higher at 13.6 V

Table 5.3: 1.5-2 ml non-coated flap elevation at four instances of current

Voltage (V)	Current (A)	Average Elevation (pixel)	Average Elevation (mm)
0	0	7.3	0.39
5.8	0.05	7.67	0.41
11.1	0.1	8	0.42
13.6	0.11	8	0.42

than the initial condition at 0 V and table 5.4 shows that the elevation in the flap is 13.5% (0.05 mm) higher at 13.6 V than its initial condition at 0 V.

When we compare table 5.1 with table 5.2 we can see that the elevation in non coated flap is 0.06 mm higher than the elevation values of the flap at maximum power suggesting that the oleophobic coat employed here has no effect on the elevation of the flap. The elevations recorded due to the electromagnet are hence very low as the required expected elevations are in the range of 0.5-2.67 mm.

Comparing tables 5.3 and 5.4 we can see the maximum variation is 0.05 mm between the initial (0 V) and final(13.6 V) condition of a coated flap which is a very low value compared to the expected value of 0.5-2.67mm as explained in A.1 to derive conclusions, since this can also be caused due to errors in edge detection calculations and minute vibrations that could've oc-

Table 5.4: 1.5-2 ml coated flap elevation at four instances of current

Voltage (V)	Current (A)	Average Elevation (pixel)	Average Elevation (mm)
0	0	7	0.37
5.8	0.05	7.3	0.39
11.1	0.1	7	0.37
13.6	0.11	8	0.42

curred during image acquisition. An increase in the magnetic field strength could provide a proper observation and hence a set of permanent magnets were used for the next experiments.

5.1.2 With permanent magnet

Since the elevation in the flap observed due to the action of the magnetic field produced by the electromagnet on the ferrofluid was insufficient to cause an elevation of at least 0.5 mm, it was decided to use permanent magnets with higher magnetic field strength. Table 5.5 shows the value of elevation in the flap at volumes of 0.5-1 ml and 1.5-2.0 ml in the presence as well as absence of a permanent **ring** magnet CS-S-18-04-N. The setup with permanent magnet employed a new platform as shown in figure A.2b. Using a new setup caused a change of plane that affected the relationship between pixel and mm as described in equation 5.1

Therefore,

$$20.66 pixels = 1 mm$$

$$1 pixel = 0.048 mm \quad (5.2)$$

For the initial volume of 0.5-1 ml a reduction in the flaps elevation by 0.02 mm is observed.

Table 5.5: Flap elevation using a Ring Magnet

Volume of ferrofluid (ml)	Elevation (pixel)	Elevation (mm)
0 ml (Initial)	7.5	0.36
0.5-1 ml (without magnet)	7	0.34
0.5-1 ml (with magnet)	6.67	0.32
1.5-2 ml (without magnet)	5.3	0.26
1.5-2 ml (with magnet)	36.67	1.77

When the volume is doubled to approximately 2 ml the elevation observed of the flap is 1.77 mm which is 392% (1.41 mm) higher than at initial condition.

Table 5.6 shows the value of elevation of the flap at volumes of 0.5-1 ml and 1.8-2.0 ml in the presence as well as absence of a permanent **disc** magnet S-20-08-N. In the case of disc magnet there is a slight elevation of 0.05 mm in the flap at 0.5-1 ml volume of ferrofluid. When the ferrofluid volume is doubled however the elevation in the flap in the presence of the magnetic field reaches to 1.89 mm, which is 456% (1.55 mm) higher than its initial position.

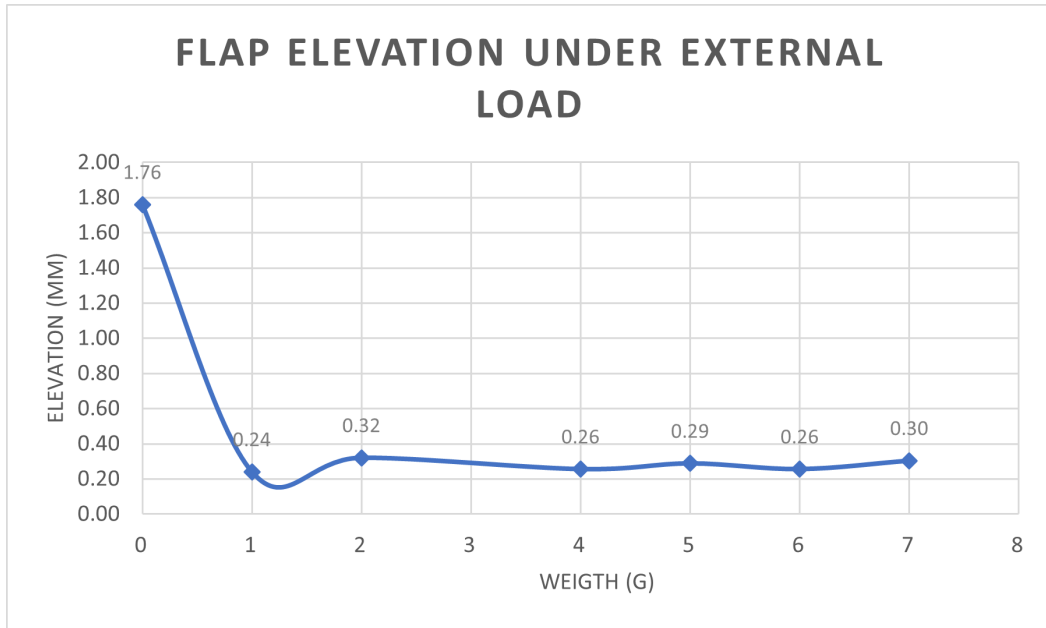


Figure 5.1: Weight(g) vs elevation(mm) of flap while using a ring magnet

It can be observed in both tables 5.5 and 5.6 that when the volume of the ferrofluid is higher, the elevation observed in the flap due to the action of the magnet on the ferrofluid is also high.

Table 5.6: Flap elevation using a Disc Magnet

Volume of ferrofluid (ml)	Elevation (pixel)	Elevation (mm)
0 ml (Initial)	7	0.34
0.5-1 ml (without magnet)	6	0.29
0.5-1 ml (with magnet)	7	0.34
1.5-2 ml (without magnet)	8	0.39
1.5-2 ml (with magnet)	39	1.89

5.2 Evaluation of force exerted by ferrofluid

Table 5.7 shows the elevation in the flap when approximately 2 ml of ferrofluid was added on the platform under the flap and a CS-S-18-04-N permanent magnet was used as described in chapter 3. Figure 5.1 also shows the weight vs elevation plot of flap elevation when a CS-S-18-04-N ring magnet is introduced under the platform. It can be seen that the graph reaches a constant level after 1 g of weight is introduced on the flap. This shows that the magnetic field strength of the CS-S-18-04-N magnet is insufficient for the ferrofluid to transfer a force sufficient enough to cause an elevation in the flap when a weight of 1 gram placed on it at a distance of 80 mm from the fixed edge.

To calculate the force exerted by the ferrofluid on the flap, following assumptions were made. The force exerted by the known load in this case 1 gram, which is 0.00981 N, is considered as a point force on the flap. The force exerted by the ferrofluid is also assumed as a point load X . The forces on the flap due to the point load results in a torque at a distance of 80 mm and 54.5

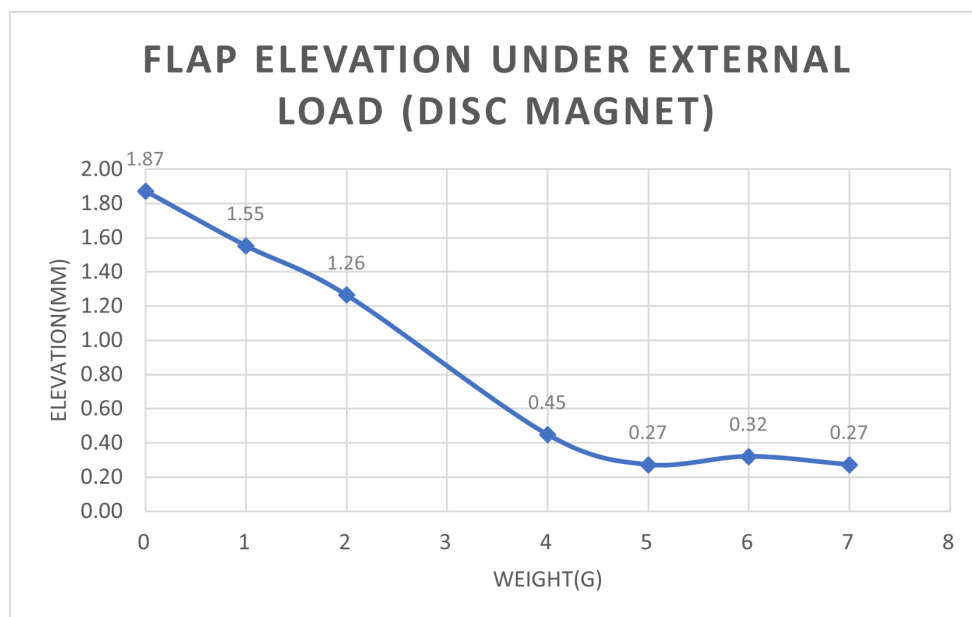


Figure 5.2: Weight(g) vs elevation(mm) of flap while using a ring magnet

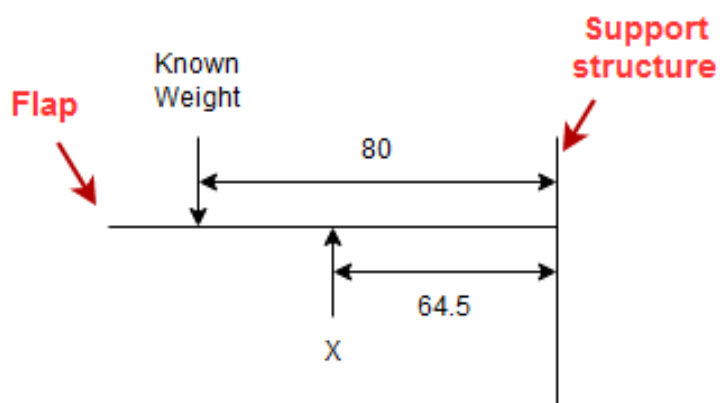


Figure 5.3: Schematic representation of forces experienced by the flap

mm respectively as depicted in figure 5.3 . The net torque is zero since the forces are acting in opposite direction and the calculation for the force is therefore given by:

For ring magnet,

$$T_1 = 0.00981 \times 80Nmm = 0.7848Nmm$$

$$T_2 = X64.5Nmm$$

$$T_1 = T_2$$

$$X = \frac{0.7848Nmm}{64.5mm}$$

$$X = 0.0122N \quad (5.3)$$

For the case of the disc magnet S-20-08-N, the elevation in the flap as observed in table 5.8

Table 5.7: Flap elevation under external load using Ring magnet

Weight (g)	Elevation (pixel)		Elevation (mm)	
	Without magnet	With magnet	Without magnet	With magnet
0 (Initial)	7	N/A	0.34	N/A
0 (Ferroidential)	6	36.67	0.29	1.76
1	6	5	0.29	0.24
2	5.67	6.67	0.27	0.32
4	6.33	5.33	0.30	0.26
5	6	6	0.29	0.29
6	6	5.33	0.29	0.26
7	5.67	6.33	0.27	0.30

Table 5.8: Flap elevation under external load using Disc magnet

Weight (g)	Elevation (pixel)		Elevation (mm)	
	Without magnet	With magnet	Without magnet	With magnet
0 (Initial)	1.67	N/A	0.08	N/A
0 (Ferroidential)	6.33	39	0.30	1.87
1	6.67	32.33	0.32	1.55
2	6	26.33	0.29	1.26
4	6.67	9.33	0.32	0.45
5	6.33	5.67	0.30	0.27
6	6.33	6.67	0.30	0.32
7	6.67	5.67	0.32	0.27

is until the weight on the flap is 5 g. This can also be seen in the plot 5.2. Using the same assumptions made in the previous case with the ring magnet here to evaluate the force we have the following:

For disc magnet,

$$T_1 = 0.049 \times 80Nmm = 3.92Nmm$$

$$T_2 = X64.5Nmm$$

$$\begin{aligned}
 T_1 &= T_2 \\
 X &= \frac{3.92Nmm}{64.5mm} \\
 X &= 0.061N
 \end{aligned}
 \tag{5.4}$$

It can be observed from the X values from equations 5.3 and 5.4 that when the magnetic field strength acting on the ferrofluid is higher the force exerted by the ferrofluid on the flap is also higher.

5.3 Model Testing

The following experiments were designed to evaluate optimum magnet position. In section 5.3.1 the results show the optimum position of the magnet on the outer surface of model-1 for maximum deflection. The change in deflection is also noted when magnetic field strength changes for the same position but with a different magnet and a different magnetic field strength. Section 5.3.2 discusses the impact of a magnet at different distances from a model. Three different models were used in this experiment. The results of the experiment are highlighted and discussed in this section.

5.3.1 Evaluation of optimum position for magnet on model surface

Table A.2 shows the deflection of the flap in model-1 with three different magnets at positions ranging from 20mm to 45mm, measured from the bottom of the case, on the outer surface of model-1 for each magnet. Since the camera used was different from previous experiments, the pixel to mm ratio also changes. The thickness of the flap was calculated using hough transform as explained in section 4.3. The flap thickness as calculated was equal to 27 pixel which is 0.5 mm. This relationship was used to obtain a relationship between pixel and mm. For this experiment therefore,

$$\begin{aligned}
 25pixels &= 0.5mm \\
 1pixel &= 0.019mm
 \end{aligned}
 \tag{5.5}$$

It can be observed in figure 5.4 that for every magnet the deflection in the flap is higher as the position of the magnet is moved towards to open end of the flap, closer to the model-1 opening. It can also be observed that stronger magnets create higher flap deflection.

5.3.2 Evaluation of optimum distance between magnet and model surface for deflection in flap

Tables A.3 and A.4 shows the deflection in the flap in model-1 and model-2 while table A.5 shows the deformation in model-3 using three different magnets at distances of the magnets ranging from 0 mm to 70 mm from the outer surface of each model.

From table 5.5 it can be observed that there is negligible deflection of the flap until the magnet approaches the 20 mm mark. In case of all three magnets at 20 mm from the model-1 surface the initial deflection in flap is observed.

Table A.4 shows the flap deflection in model-2 for different distances of three different magnets from the surface of the model. Since the flaps in this model are made of flexible TPU95A, the flaps do not deflect evenly as in the case of model-1 as can be seen figure 5.7. Due to this the point on flap furthest from the inner walls of the model-2 is considered as the deflection value of the flap. Figure 5.6 shows the plot for flap deflection at different magnet distance of 3 different magnets. In case of model-2 due to the non-uniform/uneven deflection of the flap the optimum distance of magnet cannot be clearly established as in the case of model-1. We can however see that at distance 10 mm from the model-2 surface magnet 1 and magnet 2 cause initial deflection in flap whereas magnet 3 causes an initial deflection in flap at a distance of 20 mm.

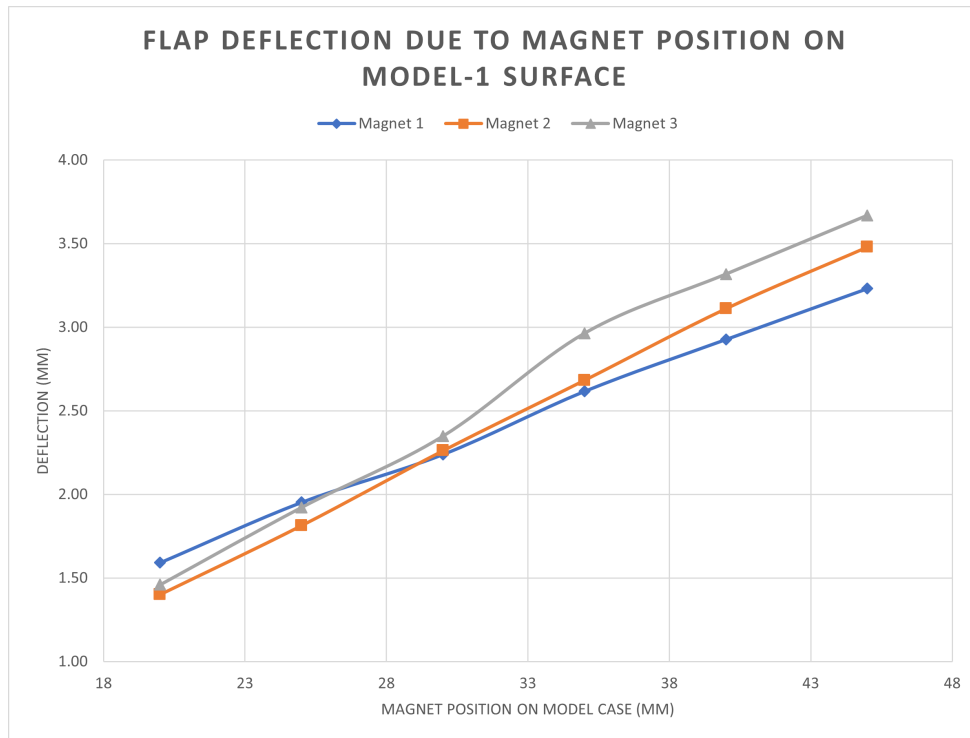


Figure 5.4: Flap deflection due to magnet position of 3 different magnets on the outer surface of model-1

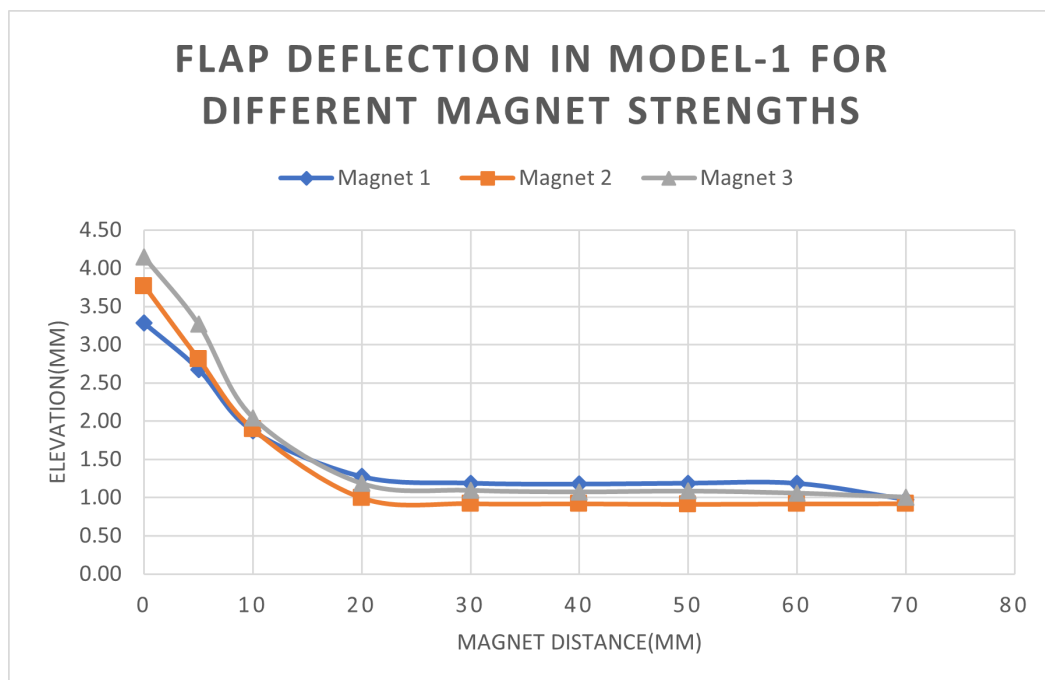


Figure 5.5: Flap deflection in model-1 for different magnet distances and strengths

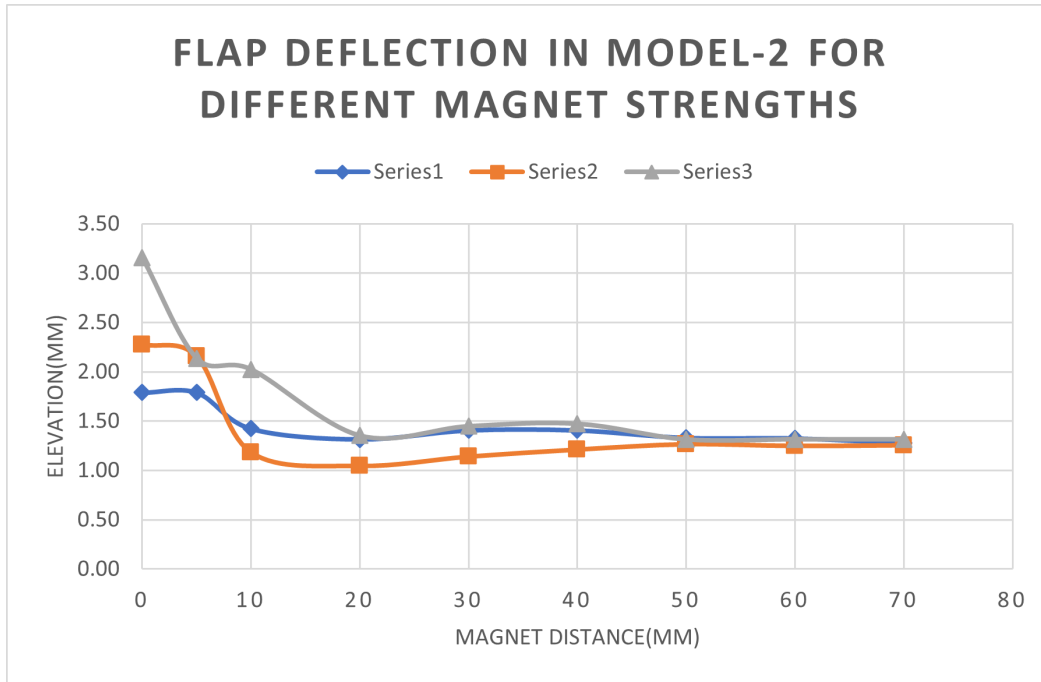


Figure 5.6: Flap deflection in model-2 for different magnet distances and strengths

When comparing figures 5.5 and 5.6 it can be observed that the maximum deflection of flap in model-1 is 131% higher when compared to the maximum deflection of the flap in model-2.

Table A.5 gives the values for deformation in the cylindrical flap. The deformations were relatively lower than the deflection values in model-1 and model-2. The maximum deformation in model-3 from the table values is 0.36 mm which is only 12% of the maximum deflection in model-1. Figure 5.8

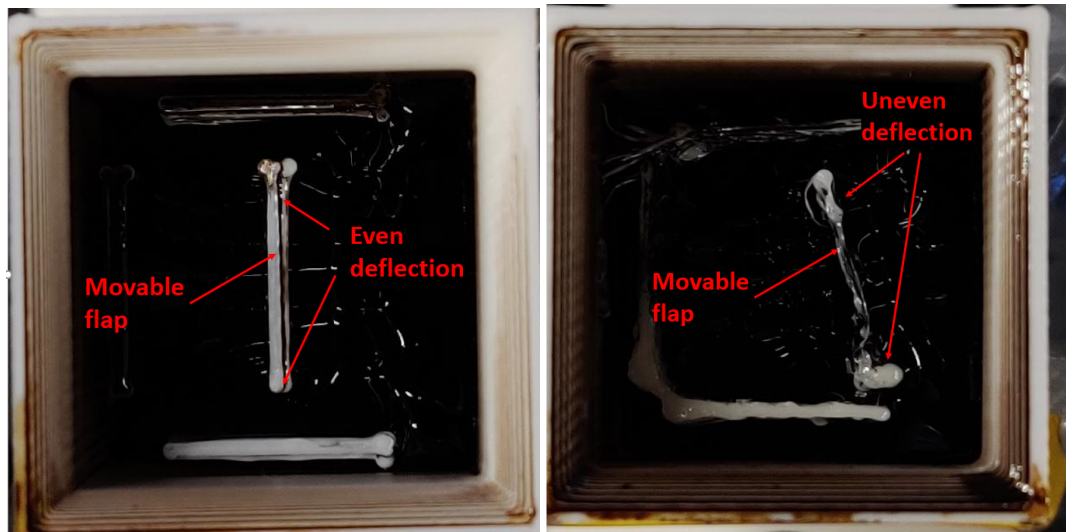
5.4 User Study

The user study was conducted to evaluate if users were able to perceive a sense of movement in the plunger and the direction of movement caused within the plunger due to model-1. The results are tabulated in two tables. Table 5.9 shows the compliance of 10 volunteers to sensing direction of bending in plunger. Table 5.10, which is a compressed version of the full table in appendix A.6, shows the compliance of the 10 volunteers with respect to various variations discussed in section 4.4.

The volunteers are said to be compliant when the movement of the plunger is sensed and the direction of the plunger sensed is the same as the direction provided to the volunteer. If a volunteer senses the movement in the plunger but in a direction that is different from the direction provided then it is characterised as incorrectly sensed. If a volunteer does not sense any movement in the plunger even after a direction was provided to the volunteer then they are recorded as "NO". All values under the column "NO" in table 5.9 indicate that the volunteers did not sense the provided direction. From table 5.9 it can be observed that the users were most compliant for the direction "UP" with a compliance percentage of 60%, which is towards the front as shown in figure 5.9. The least compliant direction sensed was "LEFT" with a compliance percentage of 29%.

68% of the times, volunteers could feel that the plunger moved. 32% of the times, the movement of the plunger was not sensed by the volunteers. 44% of the times, volunteers could sense the movement in plunger and could also tell the direction in which it was bent accurately. We can also observe that the most direction which was not sensed was the "DOWN" direction.

A very interesting observation is also made with regards to the incorrect values detected. For



(a) Flap deflection behaviour in model-1

(b) Flap deflection behaviour in model-2

Figure 5.7: Flap deflection comparison between model-1 and model-2

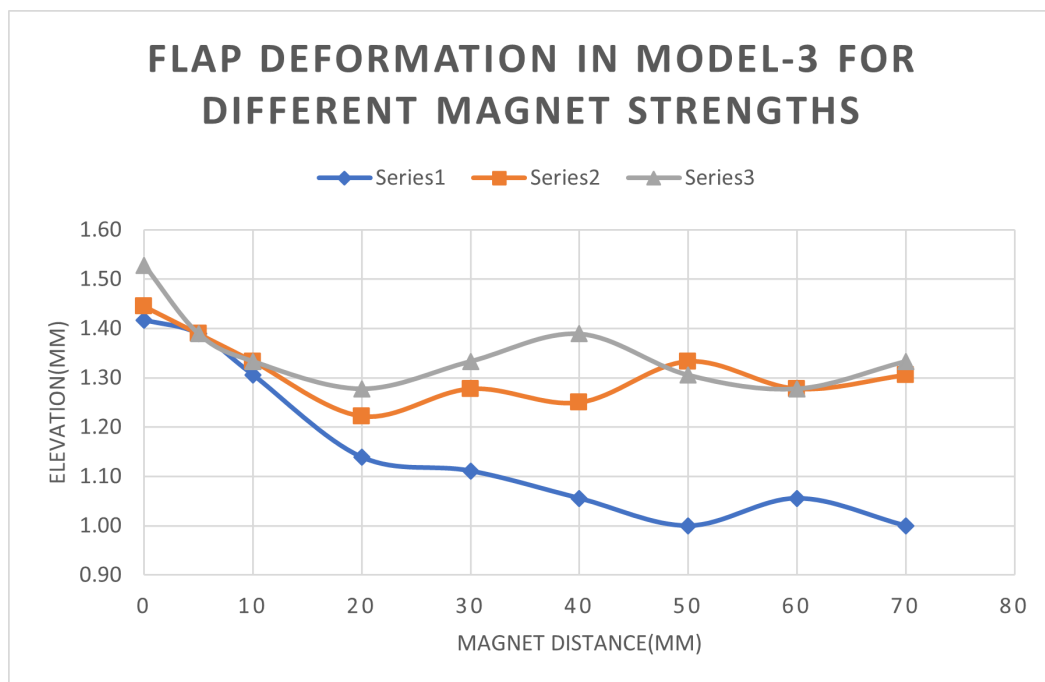


Figure 5.8: Flap deformation in model-3 for different magnet distances and strengths

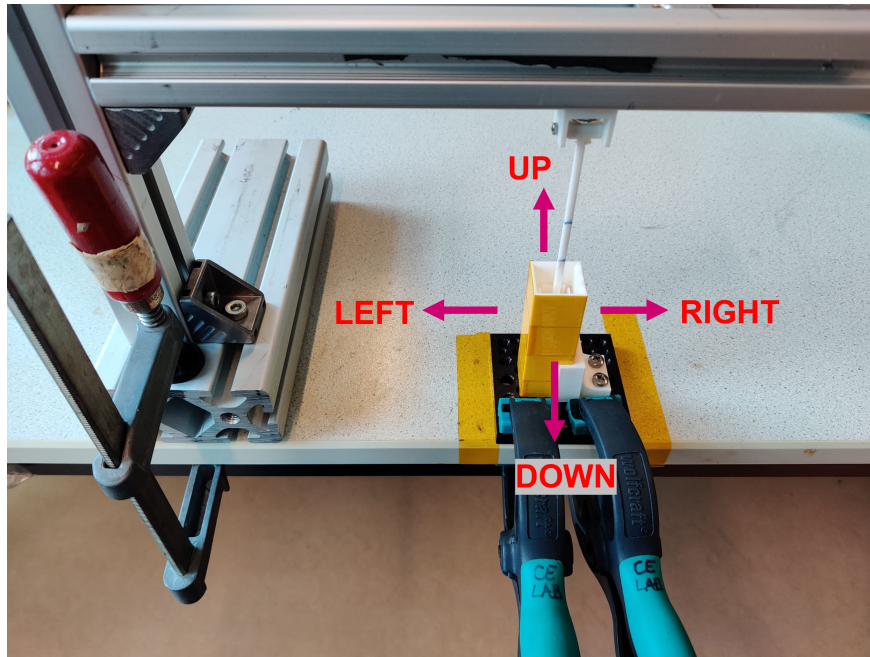


Figure 5.9: Bending direction notation of the plunger

instances, for direction provided "UP", "RIGHT" direction was sensed 18 times. Similarly for direction provided "RIGHT", "DOWN" was sensed 16 times. For direction provided "LEFT", "UP" was sensed 18 times. The only exception to this is the case when the direction provided is "DOWN". Since for direction provided "DOWN" the most incorrectly sensed direction were both "RIGHT" and "LEFT", both sensed 8 times each. Judging from the pattern from the errors above, it can be said that the error is right dominant, which means that the most incorrectly sensed direction is the direction to that of the clockwise right of the provided direction as shown in figure 5.9.

Table 5.9: Number of trials per direction provided and the corresponding direction based compliance

	Direction Sensed				Compliance			
	UP	DOWN	RIGHT	LEFT	NO	Quantity	Percentage	Not sensed (%)
UP	70	2	18	5	21	116	60%	18%
DOWN	1	30	8	8	43	90	33%	48%
RIGHT	9	16	53	0	33	111	48%	30%
LEFT	18	2	7	24	32	83	29%	39%
Total	98	50	86	37	129	400		32%

Table 5.10: Compressed compliance table for different variation

Row Labels	Total instances	Compliance (Qty)	Compliance (%)
ITCN	50	32	64%
ITON	50	31	62%
ITOA	50	24	48%
ITCA	50	24	48%
RLOA	50	19	38%
RLCN	50	17	34%
RLCA	50	16	32%
RLON	50	14	28%
Grand Total	400	177	44%

Table 5.10 shows compliance of the users based on 8 different variations listed in section 4.4. The variation ITCN (Index Thumb Closed eyes Near model) has the highest compliance value of 64%, while RLON (Ring Little finger Open eyes Near model) has the lowest compliance percentage. It can be further observed that the variation involving Index finger and Thumb have higher compliance than the Ring and Little finger.

6 Discussion

The concept designed and the distinct application of ferrofluid as developed in this thesis is novel in the context of medical feedback systems. The results of the validation experiments successfully demonstrated the feasibility of the concept by providing evidence that an elevation of a flap by ferrofluid is possible by volumetric redistribution of the ferrofluid along the magnetic field lines of a permanent magnet. An electromagnet, with magnetic properties just as the permanent magnet used in this thesis would potentially have a similar impact. The electromagnet used in the flap elevation test was relatively weak and had a small cross sectional area which made it difficult to amass the required magnetic field for volumetric redistribution in the ferrofluid to occur so as to cause an elevation in the flap which is sufficient enough for the concept discussed in chapter 3. The results of the oleophobic coating also were counter intuitive, not simply in terms of lack of elevation but the fact that the flaps covered in oleophobic coat were more stained by the ferrofluid than the non coated flap.

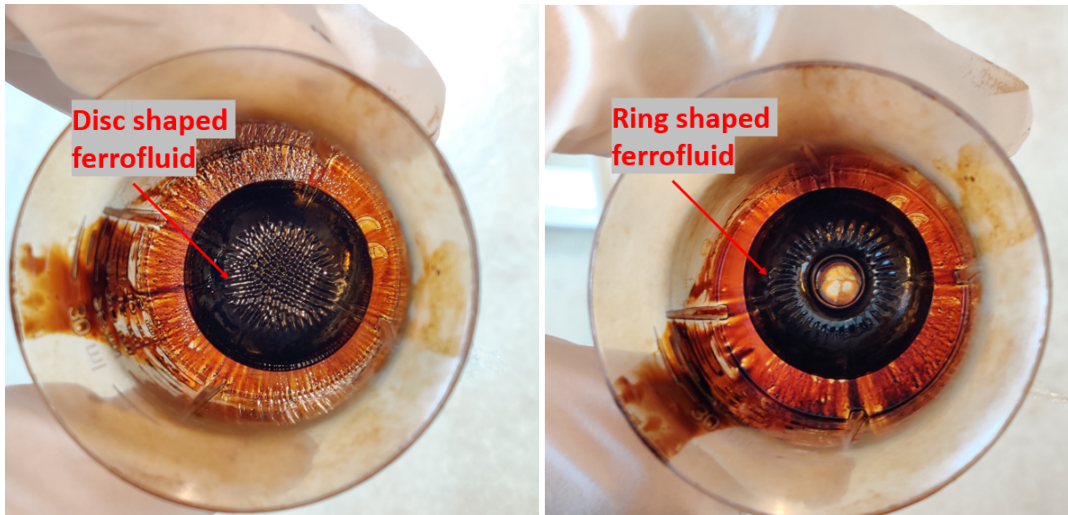
The use of permanent magnets however provided better insight about the ferrofluid behaviour under an external magnetic field. An interesting observation was the 400% rise in elevation value of the flap when ferrofluid volume was just doubled in the flap elevation test using permanent magnet. A possible cause could simply be that the additional volume of ferrofluid could only be accumulated in the same profile of the magnet. It was observed during experimentation that the ferrofluid would arrange itself in the shape of the magnetic field lines of the magnet as can be seen in figure 6.1, therefore replicating the shape of the magnet to a certain extent. This means when the additional 1 ml fluid was added, all of that fluid had to rearrange in the same given profile of the magnet which was used causing the elevation in the flap to drastically be high, up to 400% in the case of flap elevation experiment.

It was also established that ferrofluid is able to exert a force on an external entity, in this case a flap under the influence of strong magnetic field such that it could be employed in actuation based applications. The calculated loads are however a close estimation of the actual value and not the actual value itself of the force exerted by ferrofluid, since many assumptions such as the force exerted by ferrofluid was a point load, the bending of the flap was uniform bending were made.

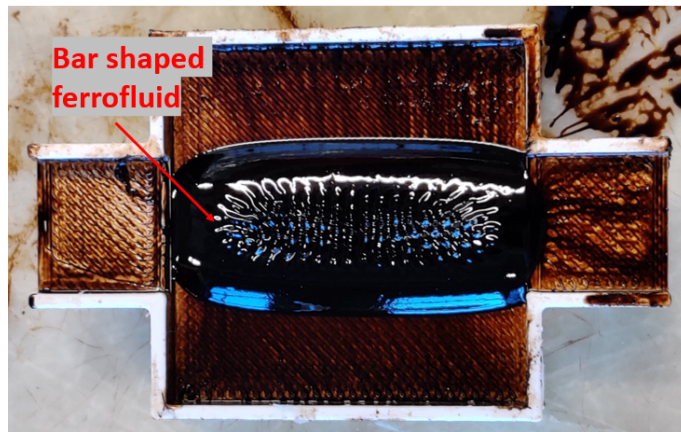
The success of the validation experiment led to designing of model-1 with white tough PLA flaps of 0.5 mm thickness to test deflection at different magnet position. The position at which a magnet would have the highest deflection was to be evaluated. Intuitively, the position closer to the face of the model would have a higher deflection as flaps were open and far away from the fixed edges on the base. However after the 45 mm mark, the ferrofluid due to the magnetic attractive force of the magnet would "jump" out of the model which would result in loss of volume and a flawed reading of deflection and hence the limit for magnet was maintained at 45 mm mark.

Another variation of model-1 was model-2 which had the same outer casing as that of model-1 but the inner flaps were composed of TPU95A. The motivation for a flexible flap was to obtain more deflection for the same force offered by the ferrofluid. However the model-2 flap provided a non-uniform deflection due to the composition of the flap itself. The cylindrical variation of model-1 was designed to mimic the cross section of a typical artery. However the flap, although composed of TPU95A, was proving to be highly resistive to deformation due to the cylindrical design of the flap. If certain vertical grooves were introduced to the cylindrical flap, The flap would be more "flexible".

The user study was conducted using model -1 since it displayed the ideal behaviour for flap deflection. While conducting the user study various observations were made. The plunger design was uniformly flexible. This made it difficult for the participants to orient the plunger in the center of the model. The plunger was also undesirably and unintentionally bent by the users



(a) Ferrofluid shape under the influence of a disc magnet (b) Ferrofluid shape under the influence of a ring magnet



(c) Ferrofluid shape under the influence of a bar magnet

Figure 6.1: Ferrofluid shapes under the influence of magnets of different shapes

towards a random direction when the holding style was changed and also when the change occurred in the variation. This incurred a "NO" response or an incorrect sense of direction from the user when the magnet was introduced. A new plunger design such that the initial part of the plunger gripped by the user can be redesigned to be more stiff and resistive to bending while the flexible part only makes contact with edge of the users hand can be seen as one way to resolve the error.

It was also observed that the speed at which the magnet was introduced towards the case for the user study also had an impact on the participants perception. If the magnet was introduced instantaneously the participant was able to perceive the direction accurately 100% of the time, however if the magnet was introduced gradually, then the participant was unable to deduce the direction correctly. In some cases participant were not able to sense any movement in the plunger at all. Since the magnet was manually being introduced, it could be the cause of many false readings as well, since the way the researcher introduced the magnet depended on the position of the researcher with respect to the setup. In this user study the researcher was positioned to the left of the setup and it caused a right bias when it came to introducing the magnet, which means that the participant felt the direction to the right of the actual direction provided more as can be observed from table 5.9. An electromagnet with similar magnetic field strength as that of a permanent magnet would resolve the issue of manual introduction of the magnet. It would also provide a magnetic field instantaneously thereby eliminating many more read-

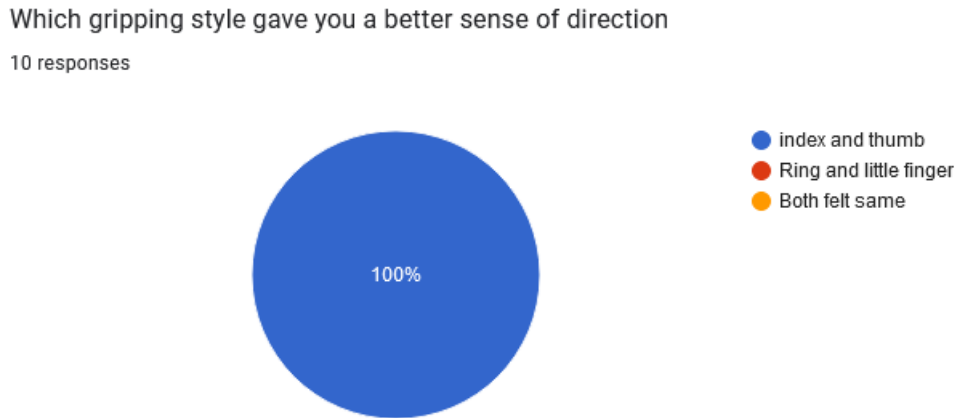


Figure 6.2: Reponse of volunteers to the question on comfortable gripping style

ings where the participants did not sense any movement in the plunger due to manual magnet introduction. The spatial orientation of the user also seemed to have an effect on the users perception of the direction of movement caused within the plunger during the user study. The users were asked to orient themselves parallel to the setup. However for practical reasons this condition was not able to be sustained and this also caused a few errors in perception of bending direction by the users.

Another interesting observation was that all the 10 volunteers answered that they felt the feedback with index finger and thumb was better than ring and little finger as seen in figure 6.2. This is also consistent with the observation made from table 5.10. Possible cause for this could be because of the vertical orientation of the setup. Since the arrangement of the model and plunger was vertical it made the holding style using ring and little finger to be difficult and unconventional. It was also observed that the participants struggled to orient the plunger in the center of the model when the plunger was gripped with their ring and little finger.

The plunger was fixed at one end but suspended in ferrofluid within the model. This caused unnecessary vibrations in the plunger as the magnetic field was being introduced to ferrofluid. This could also be one of the reasons for incorrect perception of the direction by participants. Overall while the feedback was sensed 68% of the time with an accurate sensing of direction 44% of the time, it could be possible further to minimise the error readings that occurred in the study by improving plunger design and implementing use of electromagnets.

7 Conclusion

The aim of this thesis was to develop a concept design for a ferrofluid based feedback system for the primary system of a versatile endovascular assisting robot. The development of concept was initialised based on set assumptions. A successful demonstration of the feasibility of the concept was given by the validation experiments.

The concept has been demonstrated to be functional in a vertical configuration. The basic requirements for the ferrofluid based feedback system was to provide a feedback along with a sense of direction. Based on the user study data, the ability to provide a direction based feedback was accurate to up to 44%. Although this is a low accuracy level for a feedback system of a medical telerobot, development in the plunger design along with change in the orientation of the model with adequate sealing strategy and replacement of permanent magnets with electromagnets with a control architecture will lead to the development of a feedback system which will provide a feedback that is intuitive to users in conjunction with the available haptic feedback system.

7.1 Future works

To improve the direction based feedback sensation, the plunger design must be changed in such a way that the initial part of the plunger must be stiff and only the part which comes in contact with the edge of the users palm (near the little finger) and also enters the model should be flexible and made of TPU95A. The remaining portion of the plunger which would be gripped by the user must be stiff and be made of a different component or must be reinforced to avoid bending due to user grip.

To enable a horizontal orientation of model-1 such that it replicates the envisioned concept, sealing of the model opening poses as an immediate challenge. The sealing necessary for such a model is unique as it must be flexible in nature. It must also not provide additional forces to the plunger when the plunger moves within the model. It must not provide additional forces to the movable flaps within the model. The seal should prevent ferrofluid from escaping the model and must not react with ferrofluid. Given the requirement a latex based seal was briefly explored. Figure 7.1 shows an idea of the placement for a seal as a potential solution. Dragon skin silicones, which is a silicon based sealant could be an adequate fit for the requirements of a sealant.

Electromagnets and the control architecture for the effective controlling of flaps need to be developed such that it works with an image based feedback system as in the case of CathBot(8). The requirement of the control system is such that an electromagnet must get activated when a threshold value of σ , defined as the minimum allowable distance between the catheter and the artery wall, is passed by the catheter. The added complexity is that only the electromagnet which corresponds to the directional side of catheter which is in contact with the artery wall must be activated so as to provide an accurate direction based feedback.

If the concept is commercialised the development of the working principle can be extended to various domains like the gaming industry where entire body suits filled with ferrofluid can be developed, attached with an array small electromagnets to provide a full-body haptic feedback, leading to a completely immersive gaming experience.

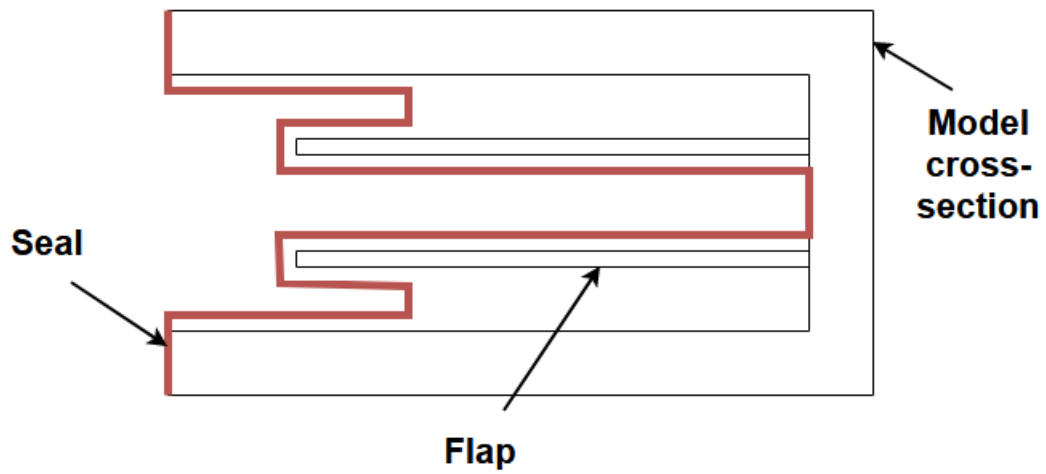


Figure 7.1: Side view cross section of model-1 with flap and seal idea

A Appendix

Matlab Code for validation and evaluation experiments

```
1
2 % read image
3 img1 = imread('weight\9.3\7mag.jpg');
4 imshow(img1)
5 %img2 = imread('c\2v.11c.jpg');
6 %figure , imshow(img2)
7
8 %convert and save
9 gryimg1 = rgb2gray(img1);
10 %gryimg2 = rgb2gray(img2);
11 %imwrite(gryimg1, 'grayimageinitialnc.png');
12 %imwrite(gryimg2, 'grayimage0.05nc.png');
13 figure , imshow(gryimg1)
14 %figure , imshow(gryimg2)
15
16 %fuse/superimpose images
17 %fused= imfuse(gryimg1,gryimg2,"blend");
18 %figure , imshow(fused)
19
20 %detect edges
21 bw1 = edge (gryimg1 , "canny",0.2,2);
22 %bw2 = edge(gryimg2,"canny",0.2,2);
23 %bw3 = edge (fused,"canny",0.2,2);
24 figure , imshow(bw1)
25 impixelinfo;
26 %figure , imshow(bw2)
27 impixelinfo;
28 %figure , imshow(bw3)
29 impixelinfo;
```

Matlab Code for model tests

```
1 %insert variable
2 %for line 1
3 x1=431;
4 x2=486;
5 y1=231;
6 y2=317;
7
8 %for line 2
9 x3=449;
10 x4=528;
11 y3=199;
12 y4=316;
13
14 m1=(y2-y1)/(x2-x1);
```

Table A.1: Technical data sheet of ferrofluid used in this thesis

Physical properties	CGS unit	SI unit
Appearance	Black-viscous	
Carrier liquid	hydrocarbonic oil	
Saturation	300 Gauss	30mT
Magnetization (Ms)	(280~350)	(28~35)
Viscosity (at 27 deg C)	80cP (30~200)	80 mPa-s (30~200)
Density (at 20 deg C)	1.04 g/ml (1.02~1.08)	1.04 g/cm ³ (1.02~1.08)
Working temperature	-20 deg C ~+130 deg C	
Freezing point	-50 deg C	
Boiling point	Over 250 deg C	
Flash point	Over 180 deg C	

```

15 %m2=abs((y4-y3)/(x4-x3));
16
17 c1=y2-(m1*x2);
18 c2=y4-(m1*x4);
19 z= sqrt(1+m1^2);
20 d= (abs(c2-c1))/z

```

Matlab Code for distance between flap and inner side of model

```

1 % read image
2 img1 = imread('cropped-picsposition 6.jpg');
3 rotimg1=imrotate(img1,33,'crop');
4 figure ,imshow(rotimg1)
5 figure ,imshow(img1)
6 impixelinfo;
7
8 %convert and save
9 gryimg1 = rgb2gray(rotimg1);
10 figure , imshow(gryimg1)
11
12 %dilate & erode image
13 se1=strel("disk",3);
14 dilimg = imdilate(gryimg1,se1);
15 se2 = strel("line",5,90);
16 eroding = imerode(dilimg,se2);
17

```

```

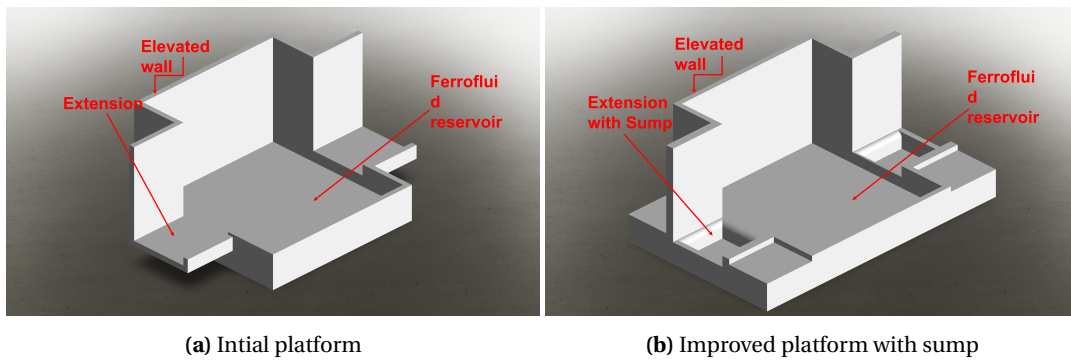
18 %detect edges
19 bw1 = edge (eroding, "canny",0.1,6);
20 %figure , imshow(bw1)
21 %impixelinfo;
22
23 %hough
24 [H,theta ,rho] = hough(bw1);
25 %figure
26 imshow(imadjust (rescale (H)) , [] , ...
27         'XData' ,theta , ...
28         'YData' ,rho , ...
29         'InitialMagnification' , 'fit ');
30 xlabel ( '\theta (degrees) ' )
31 ylabel ( '\rho ' )
32 axis on
33 axis normal
34 hold on
35 colormap (gca , hot)
36
37 P = houghpeaks (H,50 , 'threshold' , ceil (0.2*max (H (:))));
38 x = theta (P (:,2));
39 y = rho (P (:,1));
40 plot (x,y , 's' , 'color' , 'black');
41
42 lines = houghlines (bw1,theta ,rho,P , 'FillGap' ,5 , 'MinLength' ,50);
43 figure , imshow (rotimg1) , hold on
44 max_len = 0;
45 for k = 1:length (lines)
46     xy = [lines (k) .point1; lines (k) .point2];
47     plot (xy (:,1) ,xy (:,2) , 'LineWidth' ,2 , 'Color' , 'green');
48
49     % Plot beginnings and ends of lines
50     plot (xy (1,1) ,xy (1,2) , 'x' , 'LineWidth' ,2 , 'Color' , 'yellow');
51     plot (xy (2,1) ,xy (2,2) , 'x' , 'LineWidth' ,2 , 'Color' , 'red');
52
53     % Determine the endpoints of the longest line segment
54     % len = norm (lines (k) .point1 - lines (k) .point2);
55     % if ( len > max_len)
56     %     max_len = len;
57     %     xy_long = xy;
58 % end
59 end
60
61 %getpoints
62 %[ xi , yi]=getpts;
    
```

A.1 Volume of ferrofluid and required elevation

The idea behind the volume of the ferrofluid being 1 mm thick is to see the proportionality of the volume required for elevation. Given volume redistribution of ferrofluid adjusts to profile of the magnetic field lines, the expected elevation can be in the range of 0.5 ml and higher based



Figure A.1: Standard brass based weights



(a) Initial platform

(b) Improved platform with sump

Figure A.2: Different platforms

on magnetic field strength. In figure A.6 we can see volume of ferrofluid. For ideal case which is assuming ferrofluid has no internal compressive forces.

$$lbh = \pi r^2 H$$

$$H = \frac{841 \text{ mm}^2}{78.5}$$

$$H = 10.71 \text{ mm}$$

. Of course this is too high and a 1:1 volumetric relationship is assumed. Figure A.8 Shows ferrofluid behaviour under permanent magnet of diameter 20 mm. Assuming ferrofluid profile is exactly that of the permanent magnet, the expected elevation is:

$$lbh = \pi r^2 H$$

$$H = \frac{841 \text{ mm}^2}{314}$$

$$H = 2.68 \text{ mm}$$

. This is an ideal case where the fluid behaves in an ideal manner when volume is redistributed, however the attractive forces between magnet and the ferromagnetic particle within the fluid would cause compressive effect on the fluid profile resulting in the elevation to be far lesser than 2.68. Hence an expect elevation can be placed in the range of 0.5-2.5 mm.

LAMAX X7.1 Naos action camera parameters

LCD	2 inch
Waterproof	Up to 30 m
Lens	A+++ HD lens wide-angle lens at 170°
Menu languages	English, German, Czech, Slovak, Polish, Hungarian, Lithuanian
Video resolution options	4K 30 fps, 2,7K 30 fps, 1080p 60 fps, 1080p 30 fps, 720p 120 fps, 720p 60 fps
Video format	MP4
Photo format	JPG
Video codec	H.264
Photo resolution options	16 Mpix, 12 Mpix, 8 Mpix, 5 Mpix
Photo mode	Individual / burst / timer and photo time-lapse
Mains frequency	50 Hz / 60 Hz
USB devices	Micro USB 2.0
Compatibility storage	Micro SDHC up to 64 GB
Connectivity	WiFi, micro USB 2.0, HDMI
Battery capacity	900 mAh
Battery life	Full HD video at 1080p / about 90 minutes
Time to fully charge	cca. 2 hours
Compatible operating systems	Windows XP / Vista / 7 / 8 / 10, MacOS
Camera dimensions	59.2 x 41 x 29.8 mm (incl. lens)
Weight	58 g

Figure A.3: LAMAX X7.1 NAOS camera parameters

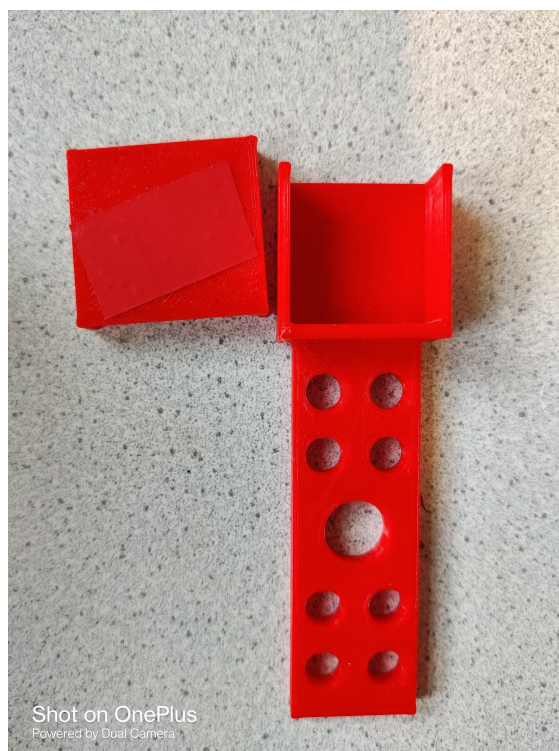


Figure A.4: Magnet case with cap used to place magnet under the platform

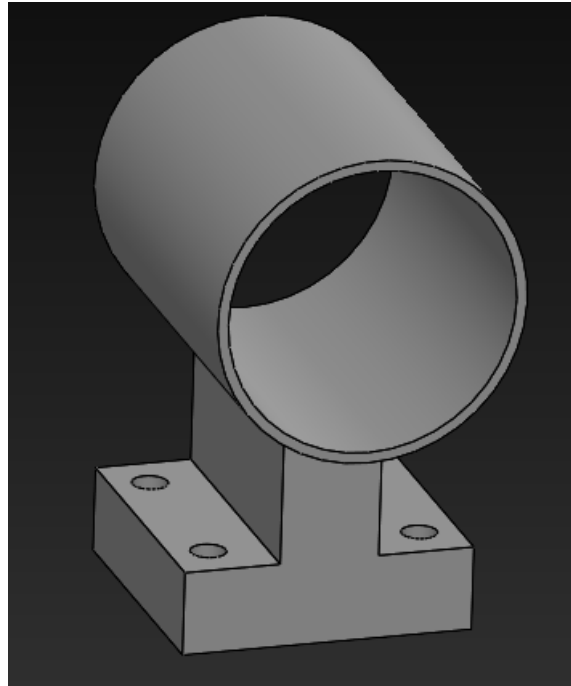


Figure A.5: Magnet holder design to be mounted on a movable trail and hold a magnet

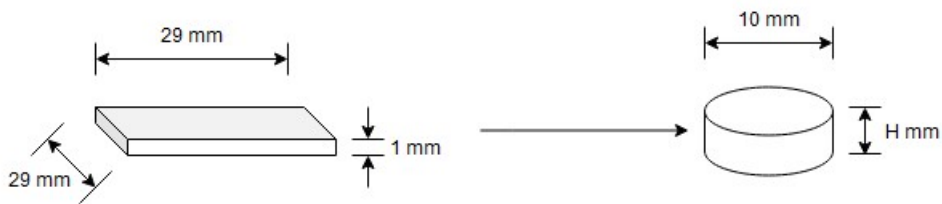


Figure A.6: Ferfluid shapes on platform. Cuboid(absence of magnetic field) and cylinder (presence of magnetic field)

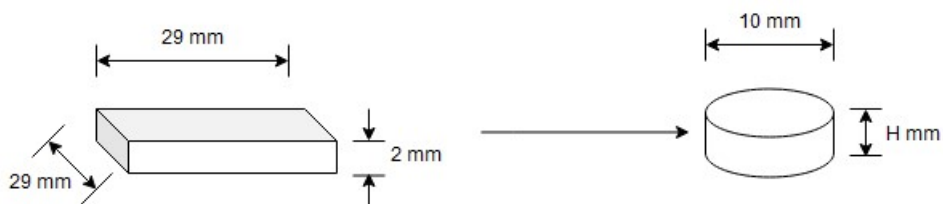


Figure A.7: Ferfluid shapes on platform. Cuboid(absence of magnetic field) and cylinder (presence of magnetic field)

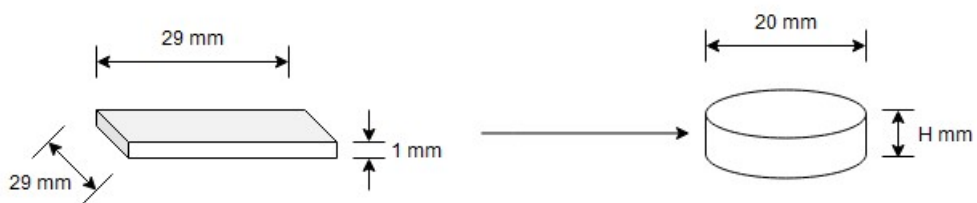


Figure A.8: Ferfluid shapes on platform. Cuboid(absence of magnetic field) and cylinder (presence of magnetic field)

Table A.2: Model-1 testing for position of magnet

Magnet	Postion	Elevation(pixels)	Elevation(mm)
Initial	N/A	46.39	0.86
Ferroinitial	N/A	67.97	1.26
Magnet 1	20	85.98	1.59
	25	105.47	1.95
	30	120.94	2.24
	35	141.31	2.62
	40	158.06	2.93
	45	174.48	3.23
Magnet 2	20	75.7	1.40
	25	97.97	1.81
	30	122.16	2.26
	35	144.88	2.68
	40	168.01	3.11
	45	187.9	3.48
Magnet 3	20	78.86	1.46
	25	103.83	1.92
	30	126.86	2.35
	35	160.04	2.96
	40	179.15	3.32
	45	198.11	3.67

Table A.3: Model-1: Impact of magnet distance on flap elevation

Magnet	Distance from surface (mm)	Elevation (pixels)	Elevation (mm)
Initial	N/A	65.79	1.32
Ferroinitial	N/A	64.19	1.28
Magnet 1	70	52.76	1.06
	60	64.12	1.28
	50	64.21	1.28
	40	63.61	1.27
	30	64.21	1.28
	20	68.86	1.38
	10	101.06	2.02
	5	144.62	2.89
Magnet 2	0	177.3	3.55
	70	49.76	1.00
	60	49.67	0.99
	50	49.35	0.99
	40	49.73	0.99
	30	49.84	1.00
	20	53.87	1.08
	10	102.49	2.05
Magnet 3	5	151.81	3.04
	0	203.55	4.07
	70	54.35	1.09
	60	57.13	1.14
	50	58.59	1.17
	40	57.99	1.16
	30	59.09	1.18
	20	63.94	1.28
10	110.42	2.21	
5	176.47	3.53	
0	223.81	4.48	

Table A.4: Model-2: Impact of magnet distance on flap elevation

Magnet	Distance from surface (mm)	Elevation (pixels)	Elevation (mm)
Initial	N/A	70.91	1.42
Ferroinitial	N/A	69.48	1.39
9.3	70	68.91	1.38
	60	71.58	1.43
	50	71.83	1.44
	40	75.94	1.52
	30	75.95	1.52
	20	71.02	1.42
	10	76.83	1.54
	5	96.6	1.93
	0	96.66	1.93
15	70	67.85	1.36
	60	67.47	1.35
	50	68.39	1.37
	40	65.46	1.31
	30	61.62	1.23
	20	56.54	1.13
	10	63.9	1.28
	5	116.39	2.33
	0	122.95	2.46
20	70	71	1.42
	60	71	1.42
	50	70.92	1.42
	40	79.51	1.59
	30	78.13	1.56
	20	73.01	1.46
	10	109.28	2.19
	5	115.41	2.31
	0	170.55	3.41

Table A.5: Model-3: Impact of magnet distance on flap elevation

Magnet	Distance from surface (mm)	Elevation (pixels)	Elevation (mm)
Initial	N/A	42	1.17
Ferroinitial	N/A	36	1.00
1	70	36	1.00
	60	38	1.06
	50	36	1.00
	40	38	1.06
	30	40	1.11
	20	41	1.14
	10	47	1.31
	5	50	1.39
	0	51	1.42
	2	70	47
60		46	1.28
50		48	1.33
40		45	1.25
30		46	1.28
20		44	1.22
10		48	1.33
3	70	48	1.33
	60	46	1.28
	50	47	1.31
	40	50	1.39
	30	48	1.33
	20	46	1.28
	10	48	1.33
	5	50	1.39
	0	55	1.53

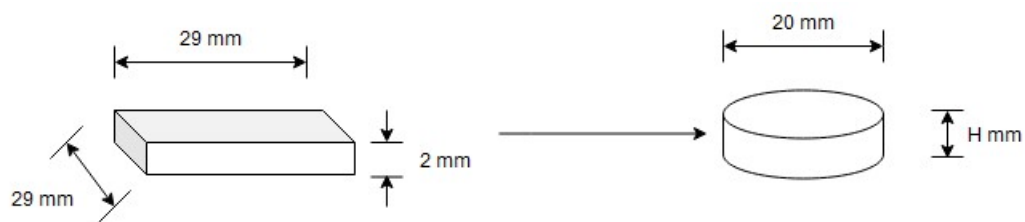


Figure A.9: Ferrofluid shapes on platform. Cuboid(absence of magnetic field) and cylinder (presence of magnetic field)

Table A.6: User-Study Data

Participant number	Variation	I	I	I	I	I	I	R	R	R	R	R	R
		1	2	3	4	5	1	2	3	4	5		
1	ITCN	UP	LEFT	LEFT	RIGHT	DOWN	NO	NO	WUP	NO	NO		
	ITON	DOWN	RIGHT	UP	RIGHT	LEFT	NO	RIGHT	UP	WDOWN	LEFT		
	RLCN	RIGHT	LEFT	UP	DOWN	RIGHT	RIGHT	LEFT	UP	DOWN	WUP		
	RLON	LEFT	RIGHT	RIGHT	DOWN	UP	NO	WDOWN	NO	NO	UP		
	ITCA	UP	DOWN	LEFT	LEFT	RIGHT	UP	WLEFT	NO	NO	RIGHT		
	ITOA	UP	UP	DOWN	DOWN	LEFT	UP	UP	UP	NO	DOWN		
	RLCA	LEFT	RIGHT	LEFT	UP	UP	WUP	WUP	WUP	WRIGHT	WLEFT		
	RLOA	DOWN	UP	DOWN	RIGHT	LEFT	NO	UP	NO	NO	WUP		
2	ITCN	UP	DOWN	LEFT	LEFT	RIGHT	WRIGHT	WLEFT	LEFT	LEFT	NO		
	ITON	RIGHT	UP	DOWN	RIGHT	LEFT	RIGHT	WLEFT	NO	RIGHT	LEFT		
	RLCN	LEFT	UP	LEFT	DOWN	RIGHT	NO	WRIGHT	NO	WLEFT	NO		
	RLON	UP	RIGHT	DOWN	RIGHT	LEFT	WRIGHT	RIGHT	NO	NO	LEFT		
	ITCA	RIGHT	LEFT	DOWN	DOWN	UP	RIGHT	LEFT	NO	WRIGHT	WRIGHT		
	ITOA	DOWN	RIGHT	UP	RIGHT	LEFT	NO	RIGHT	WRIGHT	WDOWN	LEFT		
	RLCA	LEFT	DOWN	RIGHT	UP	RIGHT	NO	WRIGHT	RIGHT	NO	RIGHT		
	RLOA	LEFT	UP	RIGHT	DOWN	LEFT	NO	WRIGHT	RIGHT	NO	NO		
3	ITCN	UP	RIGHT	DOWN	UP	LEFT	WDOWN	RIGHT	WRIGHT	UP	LEFT		
	ITON	RIGHT	LEFT	UP	RIGHT	DOWN	WDOWN	WRIGHT	UP	RIGHT	WRIGHT		
	RLCN	RIGHT	UP	RIGHT	UP	DOWN	NO	WRIGHT	NO	NO	NO		
	RLON	DOWN	RIGHT	UP	DOWN	LEFT	NO	NO	NO	NO	WUP		
	ITCA	DOWN	LEFT	RIGHT	UP	LEFT	NO	NO	RIGHT	NO	LEFT		
	ITOA	UP	UP	RIGHT	LEFT	DOWN	WRIGHT	UP	RIGHT	WUP	NO		
	RLCA	UP	LEFT	UP	RIGHT	DOWN	NO	NO	UP	NO	NO		
	RLOA	UP	RIGHT	DOWN	LEFT	UP	NO	NO	NO	NO	UP		
4	ITCN	UP	RIGHT	DOWN	RIGHT	LEFT	UP	RIGHT	DOWN	RIGHT	LEFT		
	ITON	RIGHT	DOWN	RIGHT	RIGHT	DOWN	RIGHT	NO	RIGHT	WUP	WRIGHT		
	RLCN	UP	RIGHT	RIGHT	UP	DOWN	UP	NO	WUP	WLEFT	WLEFT		
	RLON	RIGHT	DOWN	RIGHT	UP	DOWN	NO	DOWN	NO	UP	NO		
	ITCA	UP	RIGHT	LEFT	DOWN	UP	UP	WDOWN	LEFT	NO	UP		
	ITOA	RIGHT	DOWN	UP	RIGHT	UP	NO	NO	UP	WDOWN	UP		
	RLCA	RIGHT	UP	DOWN	RIGHT	LEFT	NO	WRIGHT	RIGHT	WDOWN	WRIGHT		
	RLOA	UP	LEFT	RIGHT	UP	DOWN	NO	WUP	RIGHT	NO	DOWN		

Table A.6: User-Study Data

Participant number	Variation	I	I	I	I	I	I	R	R	R	R	R	R
		1	2	3	4	5	1	2	3	4	5	1	2
5	ITCN	LEFT	RIGHT	UP	DOWN	UP	LEFT	RIGHT	UP	DOWN	UP	UP	RIGHT
	ITON	RIGHT	UP	DOWN	LEFT	RIGHT	WDOWN	UP	NO	NO	DOWN	NO	RIGHT
	RLCN	RIGHT	UP	LEFT	UP	DOWN	NO	UP	NO	NO	UP	NO	WRIGHT
	RLON	UP	RIGHT	UP	RIGHT	LEFT	UP	NO	UP	UP	WDOWN	NO	NO
	ITCA	UP	RIGHT	UP	LEFT	DOWN	UP	RIGHT	WLEFT	NO	NO	NO	NO
	ITOA	RIGHT	UP	UP	LEFT	LEFT	RIGHT	UP	NO	NO	NO	NO	NO
	RLCA	UP	RIGHT	UP	RIGHT	RIGHT	UP	RIGHT	NO	NO	NO	NO	NO
	RLOA	DOWN	UP	LEFT	RIGHT	RIGHT	NO	UP	NO	NO	RIGHT	NO	NO
6	ITCN	DOWN	UP	RIGHT	UP	LEFT	DOWN	UP	NO	UP	WUP	UP	DOWN
	ITON	LEFT	DOWN	UP	RIGHT	DOWN	LEFT	DOWN	UP	NO	DOWN	NO	DOWN
	RLCN	RIGHT	UP	DOWN	RIGHT	LEFT	RIGHT	NO	WLEFT	RIGHT	WUP	UP	DOWN
	RLON	LEFT	UP	RIGHT	UP	UP	NO	UP	WDOWN	WRIGHT	UP	UP	UP
	ITCA	RIGHT	DOWN	UP	LEFT	UP	WDOWN	DOWN	UP	LEFT	UP	UP	UP
	ITOA	RIGHT	DOWN	DOWN	UP	LEFT	WDOWN	NO	DOWN	NO	LEFT	UP	LEFT
	RLCA	LEFT	UP	LEFT	DOWN	DOWN	NO	NO	NO	DOWN	DOWN	UP	WRIGHT
	RLOA	RIGHT	LEFT	UP	DOWN	RIGHT	RIGHT	WUP	UP	DOWN	DOWN	RIGHT	RIGHT
7	ITCN	UP	RIGHT	LEFT	DOWN	RIGHT	UP	RIGHT	LEFT	DOWN	RIGHT	RIGHT	DOWN
	ITON	DOWN	UP	DOWN	LEFT	UP	NO	UP	DOWN	NO	UP	UP	DOWN
	RLCN	RIGHT	DOWN	LEFT	UP	DOWN	RIGHT	NO	WRIGHT	UP	NO	NO	DOWN
	RLON	UP	DOWN	RIGHT	DOWN	LEFT	UP	NO	RIGHT	NO	NO	NO	DOWN
	ITCA	LEFT	RIGHT	UP	UP	DOWN	LEFT	NO	UP	UP	UP	UP	DOWN
	ITOA	DOWN	UP	LEFT	RIGHT	UP	DOWN	UP	WUP	NO	UP	UP	UP
	RLCA	UP	UP	DOWN	RIGHT	LEFT	UP	WRIGHT	NO	RIGHT	WRIGHT	NO	WRIGHT
	RLOA	RIGHT	LEFT	UP	RIGHT	DOWN	NO	NO	NO	RIGHT	RIGHT	DOWN	DOWN
8	ITCN	LEFT	DOWN	RIGHT	UP	UP	WUP	DOWN	NO	UP	WRIGHT	UP	WRIGHT
	ITON	RIGHT	UP	LEFT	DOWN	DOWN	RIGHT	UP	LEFT	DOWN	DOWN	DOWN	DOWN
	RLCN	UP	LEFT	UP	RIGHT	UP	WRIGHT	WRIGHT	NO	NO	UP	UP	UP
	RLON	DOWN	UP	RIGHT	DOWN	LEFT	WRIGHT	WDOWN	NO	NO	NO	NO	WRIGHT
	ITCA	UP	UP	DOWN	UP	RIGHT	WLEFT	NO	NO	NO	NO	NO	RIGHT
	ITOA	RIGHT	DOWN	LEFT	DOWN	RIGHT	WUP	DOWN	LEFT	NO	RIGHT	RIGHT	RIGHT
	RLCA	DOWN	UP	DOWN	RIGHT	LEFT	DOWN	UP	WLEFT	NO	RIGHT	NO	RIGHT
	RLOA	LEFT	DOWN	UP	UP	RIGHT	WUP	DOWN	WRIGHT	RIGHT	UP	NO	RIGHT

Table A.6: User-Study Data

Participant number	Variation	I	I	I	I	I	I	R	R	R	R	R	R	
		1	2	3	4	5	1	2	3	4	5			
9	ITCN	DOWN	UP	RIGHT	LEFT	DOWN	DOWN	UP	RIGHT	WUP	NO			
	ITON	RIGHT	DOWN	UP	RIGHT	UP	RIGHT	DOWN	NO	NO	UP			
	RLCN	UP	LEFT	RIGHT	DOWN	RIGHT	UP	NO	RIGHT	NO	RIGHT			
	RLON	RIGHT	UP	DOWN	LEFT	RIGHT	NO	UP	WLEFT	WDOWN	NO			
	ITCA	RIGHT	LEFT	UP	RIGHT	DOWN	NO	NO	UP	NO	DOWN			
	ITOA	UP	DOWN	UP	LEFT	RIGHT	UP	NO	UP	NO	NO			
	RLCA	UP	LEFT	RIGHT	DOWN	UP	WRIGHT	NO	RIGHT	WUP	NO			
	RLOA	UP	UP	LEFT	RIGHT	DOWN	UP	WRIGHT	NO	RIGHT	NO			
	ITCN	UP	RIGHT	LEFT	RIGHT	DOWN	DOWN	UP	RIGHT	WDOWN	RIGHT	DOWN		
	ITON	DOWN	LEFT	RIGHT	UP	RIGHT	RIGHT	DOWN	LEFT	RIGHT	UP	NO		
10	RLCN	RIGHT	DOWN	UP	LEFT	RIGHT	WUP	NO	UP	WUP	RIGHT			
	RLON	DOWN	RIGHT	UP	LEFT	UP	NO	WUP	UP	WUP	UP			
	ITCA	RIGHT	LEFT	UP	RIGHT	DOWN	WDOWN	LEFT	LEFT	WDOWN	DOWN			
	ITOA	RIGHT	LEFT	LEFT	RIGHT	UP	WDOWN	LEFT	WRIGHT	WDOWN	UP			
	RLCA	DOWN	RIGHT	UP	LEFT	UP	NO	RIGHT	UP	WUP	UP			
	RLOA	RIGHT	RIGHT	UP	LEFT	DOWN	WUP	WUP	UP	WUP	NO			

Table A.7

Row Labels	Compliance Percentage of UP	Compliance Percentage of DOWN	Compliance Percentage of RIGHT	Compliance Percentage of LEFT	Total Number of Instances	Compliance Percentage	Compliance Quantity
ITCN	71%	70%	69%	46%	50	64%	32
ITON	82%	50%	59%	63%	50	62%	31
ITOA	69%	36%	31%	50%	50	48%	24
ITCA	56%	36%	42%	55%	50	48%	24
RLOA	50%	36%	62%	0%	50	38%	19
RLCN	53%	10%	44%	11%	50	34%	17
RLCA	38%	18%	67%	0%	50	32%	16
RLON	71%	8%	13%	11%	50	28%	14
Grand Total	60%	33%	48%	29%	400	44%	177

Bibliography

- [1] N. D. et al, *Dorland's Medical Dictionary for Healthcare Consumers*. Elsevier, 2007.
- [2] H. Ritchie and M. Roser, "Causes of death," *Our World in Data*, 2018. <https://ourworldindata.org/causes-of-death>.
- [3] D. T. Jamison, J. G. Breman, A. R. Measham, G. Alleyne, M. Claeson, D. B. Evans, P. Jha, A. Mills, and P. Musgrove., *Disease Control Priorities in Developing Countries, 2nd edition*. The International Bank for Reconstruction and Development, 2006.
- [4] M. Azizian, M. Liu, I. Khalaji, and S. DiMaio, *The Da Vinci Surgical System*. 2017.
- [5] Nanavati, A. J., and S. Nagral, "Why have we embraced minimally invasive surgery and ignored enhanced recovery after surgery?," 2016.
- [6] C. W. Kim, Y.-P. Lee, W. Taylor, A. Oygur, and W. K. Kim, "Use of navigation-assisted fluoroscopy to decrease radiation exposure during minimally invasive spine surgery," *The Spine Journal*, vol. 8, no. 4, pp. 584–590, 2008.
- [7] R. H. Taylor, A. Menciassi, G. Fichtinger, P. Fiorini, and P. Dario, *Medical Robotics and Computer-Integrated Surgery*, pp. 1657–1684. Cham: Springer International Publishing, 2016.
- [8] D. Kundrat, G. Dagnino, T. Kwok, M. Abdelaziz, W. Chi, T. Nguyen, C. Riga, and G. zhong Yang, "An mr-safe endovascular robotic platform: Design, control, and ex-vivo evaluation," *IEEE transactions on biomedical engineering*, vol. 68, pp. 3110–3121, Oct. 2021. Publisher Copyright: CCBY Funding Information: This work was supported by the U.K. EPSRC under Grant EP/N024877/1 Publisher Copyright: © 1964-2012 IEEE.
- [9] J. Peirs, J. Clijnen, D. Reynaerts, H. V. Brussel, P. Herijgers, B. Corteville, and S. Boone, "A micro optical force sensor for force feedback during minimally invasive robotic surgery," *Sensors and Actuators A: Physical*, vol. 115, no. 2, pp. 447–455, 2004. The 17th European Conference on Solid-State Transducers.
- [10] M. E. M. K. Abdelaziz, D. Kundrat, M. Pupillo, G. Dagnino, T. M. Y. Kwok, W. Chi, V. Groenhuis, F. J. Siepel, C. Riga, S. Stramigioli, and G.-Z. Yang, "Toward a versatile robotic platform for fluoroscopy and mri-guided endovascular interventions: A pre-clinical study," in *2019 IEEE/RSJ International Conference on Intelligent Robots and Systems (IROS)*, pp. 5411–5418, 2019.
- [11] P. Henny, *Challenges of building haptic feedback for surgical robots*. WTWH Media LLC, 2019.
- [12] T. Sheridan, "Telerobotics," *Automatica*, vol. 25, no. 4, pp. 487–507, 1989.
- [13] Sheridan, "Mit research in telerobotics," 1987.
- [14] W. Mugge, J. Schuurmans, A. C. Schouten, and F. C. T. van der Helm, "Sensory weighting of force and position feedback in human motor control tasks," *Journal of Neuroscience*, vol. 29, no. 17, pp. 5476–5482, 2009.
- [15] NimaNajmaei, *Design of a Haptic Interface for Medical applications using MRF based Actuators*. Dept. of electrical and computer engineering, University of Western Ontario, 2014.
- [16] R. Blenkinsopp, *What is Haptic feedback*. Ultraleap, 2019.
- [17] A. Khanicheh, D. Mintzopoulos, B. Weinberg, A. A. Tzika, and C. Mavroidis, "Evaluation of electrorheological fluid dampers for applications at 3-t mri environment," 2008.
- [18] J. E. Stangroom, "Electrorheological fluids," *Physics in Technology*, vol. 14, pp. 290–296, nov 1983.

- [19] A. Olabi and A. Grunwald, *Design and application of magnetorheological fluid "MRF"*. School of mechanical engineering and manufacturing engineering, Glasnevin, Ireland.
- [20] C. Scherer and A. F. Neto, "Ferrofluids: properties and applications," *Brazilian Journal of Physics*, 2005.
- [21] L. Vékás, "Ferrofluids and magnetorheological fluids," in *Advances in science and technology*, vol. 54, pp. 127–136, Trans Tech Publ, 2008.
- [22] MATLAB, *version 7.10.0 (R2010a)*. Natick, Massachusetts: The MathWorks Inc., 2010.
- [23] S. Brodoehl, C. M. Klingner, and O. W. Witte, "Eye closure enhances dark night perceptions," *Scientific reports*, vol. 5, no. 1, pp. 1–10, 2015.
- [24] D. Goldreich and I. M. Kanics, "Tactile acuity is enhanced in blindness," *Journal of Neuroscience*, vol. 23, no. 8, pp. 3439–3445, 2003.